Space Weather

RESEARCH ARTICLE
10.1029/2022SW003155

Key Points:

- The new Model for Atmospheric Ionising Radiation Effects (MAIRE+) is presented
- MAIRE+ uses neutron monitor data, sunspot number, Kp, and geostationary proton flux to nowcast the aviation radiation environment
- Model outputs are compared to data from a solid-state detector carried on board Concorde during ground level enhancements in 1989

Correspondence to:
A. D. P. Hands,
a.hands@surrey.ac.uk

Citation:
Hands, A. D. P., Lei, F., Davis, C. S., Clewer, B. J., Dyer, C. S., & Ryden, K. A. (2022). A new model for nowcasting the aviation radiation environment with comparisons to in situ measurements during GLEs. *Space Weather*, *20*, e2022SW003155. https://doi.org/10.1029/2022SW003155

Received 13 MAY 2022
Accepted 2 JUL 2022

A New Model for Nowcasting the Aviation Radiation Environment With Comparisons to In Situ Measurements During GLEs

A. D. P. Hands[1], F. Lei[1], C. S. Davis[1], B. J. Clewer[1], C. S. Dyer[1,2], and K. A. Ryden[1]

[1]Surrey Space Centre, University of Surrey, Guildford, UK, [2]CSDRadConsultancy, Fleet, UK

Abstract Significant increases to the atmospheric radiation environment are recorded by a network of ground level neutron monitors as ground level enhancements (GLEs). These space weather phenomena pose a risk to aviation via single event effects in aircraft electronics and ionizing dose to passengers and crew. Under the UK Space Weather Instrumentation, Measurement, Modeling and Risk programme, we have developed a new model to provide nowcasts of the aviation radiation environment, including both the galactic cosmic ray (GCR) background and during GLE events. The Model for Atmospheric Ionising Radiation Effects (MAIRE+) uses multiple data sources to characterize primary GCR and GLE particle spectra and combines these with precalculated geomagnetic and atmospheric response matrices to predict particle fluxes from ground level to 20 km altitude across the entire globe. Two European neutron monitors (located at Oulu in Finland and Dourbes in Belgium) are used as the primary indicators of GLE intensity in order to maximize accuracy over UK airspace. Outputs from MAIRE+ for the historical GLEs in September and October 1989 are compared to recalibrated empirical data from a solid-state detector that was carried on Concorde in that period. The model will be hosted in the UK and will provide additional capability to the Met Office Space Weather Operations Center (MOSWOC).

Plain Language Summary Ionizing radiation in the atmosphere is primarily caused by galactic cosmic rays (GCR) interacting with the upper atmosphere, creating showers of secondary radiation. At aviation altitudes the radiation environment is hundreds of times more intense than that experienced at the ground level. This relatively stable background level of radiation is punctuated by space weather events called ground level enhancements (GLEs), when energetic solar protons arrive at Earth and lead to elevated atmospheric radiation levels that can be orders of magnitude greater than background levels. Under the UK Space Weather Instrumentation, Measurement, Modeling and Risk programme, we have developed a new model to provide nowcasts of the aviation radiation environment, including both the GCR background and during GLE events. Through our Model for Atmospheric Ionising Radiation Effects, we show how data from ground level neutron monitors can be used to characterize the atmospheric radiation environment from ground level to 20 km altitude across the entire globe.

1. Introduction

The atmospheric ionizing radiation environment is relatively stable for the great majority of the time, varying in intensity in anticorrelation with solar activity over the 11 year solar cycle. The source of this ionizing radiation is interactions between galactic cosmic rays (GCR) with molecules in the upper atmosphere, which leads to secondary cascades of various particle species, of which neutrons are of primary importance. This quiescent background environment is punctuated by both increases and decreases in measurable quantities such as particle flux and dose rate during periods of high solar activity (such fluctuations are thus manifestations of space weather). Magnetic disturbances in the heliosphere, due to coronal mass ejections and corotating interaction regions of the solar wind, can lead to so-called Forbush decreases in the counting rates of ground level neutron monitors (Lockwood, 1971; Lockwood et al., 1991). These tend to manifest as rapid drops in intensity of the order of a few percent (up to a maximum of about 32% in June 1991), followed by a slower recovery that can take several days, weeks, or even months to return to the level prior to the event. Enhancements to the background environment can also occur over a range of timescales. Geomagnetic storms can reduce the geomagnetic cut-off rigidity at a given location, leading to small enhancements in incident cosmic ray intensity and thus the atmospheric radiation environment. This particularly affects midlatitude locations, which are more sensitive to small changes in rigidity. Of greater

significance, however, are the much larger increases that can be caused during solar energetic particle events (SEPEs). Unlike Forbush decreases and geomagnetic storm enhancements, these are not the consequence of a modulation in the intensity of cosmic rays, but rather they are the result of high energy solar protons (and to a lesser extent alpha particles and heavy ions) emitted from the Sun in the direction of the Earth. When SEPEs occur with sufficient intensity and energy they can lead to ground level enhancements (GLEs) in the radiation level at the Earth's surface (as measured by neutron monitors). Since the 1940s a total of 73 GLEs have been recorded, at an average rate of approximately one per year (Karapetyan, 2008; Usoskin et al., 2016).

This article describes the development of an improved Model for Atmospheric Ionising Radiation Effects (MAIRE+) developed under the UK Space Weather Instrumentation, Measurement, Modeling and Risk (SWIMMR) programme to provide real-time information to the aviation sector via the UK Met Office. Model outputs include particle fluxes, dose rates and, uniquely, single event effects (SEEs) in electronics, which are known to affect avionics (Normand & Baker, 1993; Taber & Normand, 1993) as well as ground systems (Dyer et al., 2020; Normand, 1996). MAIRE+ is an operational model that calculates radiation levels during both GCR and GLE conditions. During a GLE, these are summed to produce the total radiation environment. In quiet periods, which represent the vast majority of the time, the model produces GCR-induced radiation only. The data sources underlying each of these modes are described separately below. In both cases ground level neutron monitors are important, but in the case of GLEs they are indispensable.

2. Galactic Cosmic Rays (GCR)

The intensity of GCR varies inversely with solar activity. The modulation of cosmic rays can be derived from sunspot numbers using the method described by Nymmik et al. (1992). This method was adopted into the ISO-15390 standard model for GCRs (ISO, 2004) and has been implemented into MAIRE+ to provide continuity with predecessor models QARM (Lei et al., 2004) and MAIRE (Hands et al., 2017). However, the ISO approach, like others based on heliocentric potential modulation parameters with a monthly cadence (O'Neill, 2010), cannot recreate variations on a finer timescale such as Forbush decreases. We have therefore included an additional cosmic ray model in MAIRE+, which is able to achieve much finer time resolution. By simplifying the ISO model and linking the GCR modulation parameter to space-based heavy ion flux measurements, the German Aerospace Center (DLR) have created a model that gives better agreement with empirical data (Matthiä et al., 2013). Furthermore, the DLR model bypasses the need to drive the model directly with heavy ion data by correlating heavy ion flux with neutron monitor count rates on the ground. This extends the timeframe for historical comparison and means that the only data required by MAIRE+ to produce primary GCR fluxes is the count rate from the Oulu ground level neutron monitor (https://cosmicrays.oulu.fi/). Although the validation of this process is based on count rates averaged over 27 day Bartels rotation periods, by making the reasonable assumption that fluctuations in pressure-corrected neutron monitor count rates over shorter timescales are also directly linked to cosmic ray intensity, we achieve a much finer time resolution when implementing this model in MAIRE+. By using both the international sunspot number (ISSN) and count rates from Oulu neutron monitor, MAIRE+ incorporates two GCR models to derive primary background spectra for protons and alpha particles ($Z = 1$ and 2). The calculation of atmospheric neutron radiation requires the additional stages of transporting particles through the magnetosphere and atmosphere, which is also achieved for heavy ions up to $Z = 28$ by scaling the alpha response by abundance ratio and nucleon number.

Particle fluxes at the top of the atmosphere are calculated by applying a rigidity cut-off (for an assumed vertical arrival direction) to the primary GCR spectrum at all geographical locations. Cut-off rigidity as a function of longitude and latitude is calculated using Planetocosmics particle trajectory simulations (Desorgher et al., 2006) with the IGRF-13 internal magnetic field model (Alken et al., 2021) and the Tsyganenko external field model (Tsyganenko, 1989). The Tsyganenko '89 model uses the planetary Kp index as a measure of geomagnetic activity. Vertical cut-off rigidity maps are precalculated at 5 year IGRF epochs (from 1955 to 2020) at 100 km altitude, with interpolation between epochs calculated using invariant magnetic coordinates (at the correct date) and disturbance index. An extension to the Tsyganenko model is applied to extend the valid Kp range up to Kp = 9 (Boberg et al., 1995). An example rigidity cut-off map is shown in Figure 1.

Particle fluxes in the atmosphere are calculated using response matrices based on particle transport calculations with FLUKA (Battistoni et al., 2007). Response matrix simulations use a layered atmospheric model based on

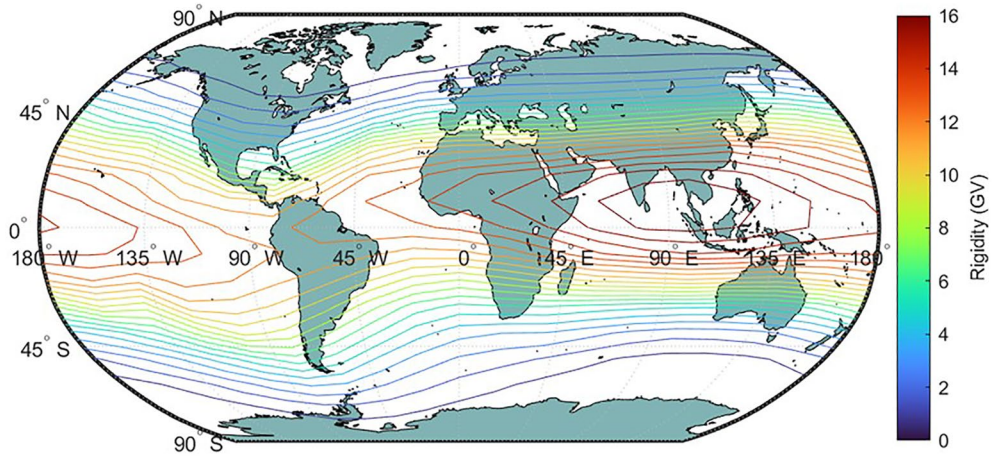

Figure 1. Contour map showing vertical cut-off rigidity at Kp = 0 (calculated at 12/09/2007).

NRLMSISE-00 to produce secondary particle spectra as a function of altitude for a series of monoenergetic incident cosmic rays. Dose rates (including ambient dose equivalent and effective dose) are calculated from these particle spectra using established fluence-to-dose conversion factors for both effective dose (ICRP 116, Petoussi-Henss et al. (2014)) and ambient dose equivalent (Pelliccioni, 2000). The overall dose rate at a particular point in the atmosphere is simply a summation of the contributions from different secondary particle species. SEE rates are included in the output using representative device cross sections for neutron-induced single event upset (SEU) and single event latch-up (SEL). This is the same methodology that was used in the predecessor models to MAIRE+: QARM (Lei et al., 2004, 2006) and the original (static) MAIRE model (http://maire.uk).

3. Ground Level Enhancements (GLEs)

The GLE model in MAIRE+ is independent of the GCR model in terms of its triggering conditions and operation but uses the same methodology to calculate radiation environment quantities in the atmosphere (flux, dose, etc.) based on a primary input spectrum. As with the GCR model, the primary spectrum is first transported through a magnetospheric model, which varies according to the geomagnetic Kp index. Only protons are included in the primary spectrum, as GLEs have a smaller and far more unpredictable heavy ion component compared to GCRs. Once the transported primary spectrum has been calculated at the top of the atmosphere (as a function of cut-off rigidity for each geographic location), the same response functions for calculating particle fluxes and dose rates are used as for the GCR model.

Unlike the GCR model, which simply modifies a well-defined primary spectrum using a single modulation parameter, there is no single spectral shape that can be applied to all GLEs. Attempts to characterize the spectral shape of GLEs have taken various forms, including Weibull functions (Dyer & Lei, 2001; Dyer et al., 2003), double-power-law "Band" functions (Asvestari et al., 2017; Atwell et al., 2011; Band et al., 1993; Tylka & Dietrich, 2009), and modified power-laws (Jiggens et al., 2019; Mishev et al., 2014; Mishev & Usoskin, 2016). These may be parameterized as functions of energy or rigidity, but the essential difference remains the slope of the spectra (spectral index) in the region of interest for atmospheric radiation effects–that is, particle rigidities from ~1 GV to >10 GV.

3.1. Spectral Determination

Knowledge of the primary proton spectrum for a GLE can be acquired directly from space-based detectors (Copeland, 2018; Jiggens et al., 2019) or indirectly from ground level neutron monitors (Miroshnichenko, 2018; Usoskin et al., 2016). The former data source is inadequate on its own due to the limited energy range, which extends only up to hundreds of MeV. However, the latter is also problematic as the extraction of the spectrum requires taking into account the response functions of the detectors (Clem & Dorman, 2000) and their energy-dependent viewing directions at the time of the event (Danilova et al., 1997; Storini et al., 2001)–often

Figure 2. Neutron monitor station locations in Northern Europe (Note: the Zugspitze neutron monitor has closed but a Bonner Sphere Spectrometer detector remains at the site). Map sourced from nmdb.eu.

combined to create a "yield function" specific to each location (Nuntiyakul et al., 2020). Comprehensive analyses of the spectral characteristics of GLEs can include data from dozens of neutron monitors in order to extract multiple parameters, including those relating to the anisotropy of the event, which, like the spectral shape, varies with time. This global modeling is a complex unfolding process that requires a lot of computing power to operate in real time. The Japanese WASAVIES model currently uses a simplified algorithm with data from several neutron monitors to achieve global modeling for an operational service (Sato et al., 2018). However, studies have shown even estimates based on very similar methodologies can produce differences of up to an order of magnitude in the assessment of radiation environment intensity at aircraft altitudes (Bütikofer & Flückiger, 2013, 2015). For example, three separate analyses of the aircraft radiation environment during GLE60 (on 15 April 2001) produced dose rates varying from a few microsieverts per hour to over 40 microsieverts per hour on two transatlantic flights (Bombardieri et al., 2007; Matthiä et al., 2009; Plainaki et al., 2010). Measurements from detectors on these flights peaked at approximately 7–9 microsieverts per hour above the GCR background (Beck et al., 2008).

Simplified approaches include applying a range of spectral shapes to bound the upper and lower potential extremes of the radiation environment (Latocha, 2018), using high latitude monitors in combination with semi-empirical rigidity and altitude functions (Lantos & Fuller, 2004) or simply using the peak measured neutron monitor increase as a proxy for the maximum likely dose rate at a given altitude (Mishev et al., 2018). For MAIRE+ we chose to take a balanced approach between accuracy and simplicity for rapid calculations. Previous work has shown that it is possible to infer spectral information for a GLE using only two neutron detectors based on the ground, provided there is sufficient spread in the cut-off rigidity of the two locations (Hands et al., 2021). This is achieved by comparing the relative increases at the two different locations to a model prediction as a function of spectral index (and is thus valid worldwide only if isotropy is assumed). In order to minimize uncertainties due to any potential early phase anisotropy effects and reflecting the focus of MAIRE+ on UK airspace, we only considered neutron monitors from European stations to form the basis of the spectral determination. Figure 2 shows a map of current European neutron monitor stations (some of which host more than one detector).

The geomagnetic cut-off rigidities for the station locations are given in Table 1. Only one station close to UK airspace, Oulu (Finland), has a cut-off rigidity below 2 GV. In order to capture relatively soft spectrum GLE events it is essential that one of the two stations used in our calculation is at high latitude, with a cut-off below 1 GV. Therefore, Oulu data are automatically selected for ingestion into our analysis. Any location with a cut-off rigidity in the range 0–1 GV is, to a first approximation, equivalent to any other in that range as the upper value corresponds to the energy threshold for production of the secondary neutron cascades that penetrate to aviation altitudes (Shea & Smart, 1990). Furthermore, data from Oulu (which extend back to 1964) have been shown to be very stable and suitable for scientific use (Mishev et al., 2020). As Oulu is close to sea level, it does not suffer from the complications introduced by snowfall at high altitude neutron monitor locations. Nor is it affected by the erratic behavior that is visible in long-term data sets from some other stations.

Table 1
Coordinates and Vertical Cut-Off Rigidities for Selected Neutron Monitor Stations

Station	Latitude	Longitude	Rigidity (GV)	Altitude (m)
Oulu	65.05	25.47	0.5	15
Kiel	54.34	10.12	2.1	54
Dourbes	50.1	4.6	3.0	225
Lomnicky Stit	49.2	20.22	3.5	2,634
Jungfraujoch	46.55	7.98	4.2	3,475

Note. Rigidity cut-off is calculated by the MAIRE model for November 2021 using a fixed geomagnetic Kp index of two and an altitude of 20 km.

To minimize uncertainty when comparing the relative increases at different neutron monitor locations, we prefer to select monitors at similar altitudes to each other. This rules out the high altitude stations at Lomnicky Stit and Jungfraujoch, even though their high altitude locations do compensate somewhat for the higher cut-off rigidities compared to Kiel and Dourbes. Comparisons between data from Kiel and Dourbes revealed an instability in the count rate for the former which renders it unsuitable for MAIRE+. The cause of the fluctuating count rate at Kiel is unexplained, but users are advised not to use the data for scientific purposes (nmdb.eu). We therefore established the pairing of Oulu and Dourbes neutron monitors as the basis for spectral shape determination. This has the added advantage that both stations are of the

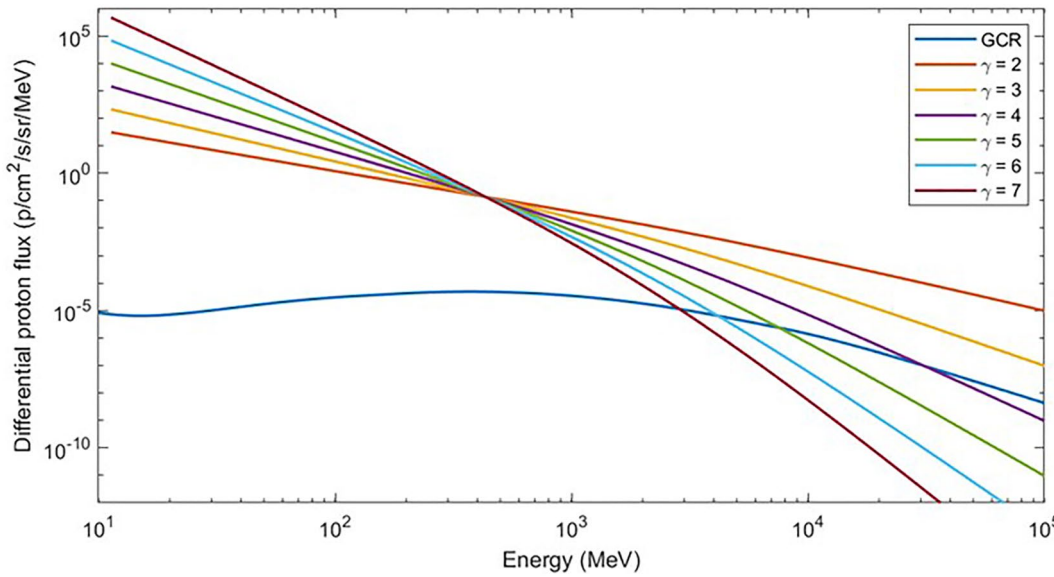

Figure 3. GLE proton spectra as a function of rigidity spectral index, transformed into energy for comparison with the GCR background. The normalization of the GLE spectra is arbitrary as the intention is to compare shape only. Only proton energies greater than ~350 MeV affect the radiation environment at aircraft altitudes.

same type: a 9-tube NM64 design filled with BF_3 gas for thermal neutron detection (Hatton & Carimichael, 1964; Kananen et al., 1991). In all cases we use count rates that have been corrected at source for pressure variation and detector efficiency (Paschalis & Mavromichalaki, 2013). For reasons of real-time processing efficiency, we do not attempt to apply a differential pressure correction during GLE periods, where different correction factors may be applied separately to estimated GCR and GLE components using the two-attenuation length method described by McCracken (1962). As Oulu and Dourbes are both low altitude stations the correction to constant pressure (1000 mbar) is less than it would be for high altitude stations (we calculate that applying the two-attenuation length method to neutron monitor data from the 1989 GLE examples shown in this article would adjust estimated GLE-component count rates by only 2%–3%).

As we are using a simplified two-station approach to infer spectral information, it is appropriate to use a simple function as the basis of the spectral shape. We assume a single power law in rigidity (P) to describe the differential proton flux outside the magnetosphere (Equation 1).

$$J(P) = J_0 P^{-\gamma} \tag{1}$$

Where γ is the spectral index and J_0 is the normalization parameter for differential flux (in units of protons/cm^2/s/sr/MeV). This spectral form is adequate for describing the >1 GV part of a GLE spectrum, though it should not be used to extrapolate to lower rigidities/energies as this would require a Band function or modified power law (as described earlier) in order to reflect the lower gradient observed below the knee in the spectrum where space-based measurements are used (Jiggens et al., 2019; Tylka & Dietrich, 2009). Figure 3 shows these spectra transformed into functions of energy and compared to the GCR background.

Using the radiation transport response functions within the static MAIRE model (Hands et al., 2016), together with NM64 response functions (Clem & Dorman, 2000), we calculated count rates at Oulu and Dourbes for the GCR background and GLE conditions as a function of spectral index in discrete steps in the range $\gamma = 2$–7. The absolute values we calculated for GCR conditions using omnidirectional neutron spectra were slightly (~40%) higher than those recorded by the 9-NM64 monitors, but the difference is possibly caused by attenuation by the buildings containing the monitors (which we did not factor in) and the uncertainty introduced by the fact that response functions are given assuming normal incidence, whereas a more isotropic distribution is expected at ground level. In any case, an absolute count-rate discrepancy is unimportant as we are calculating the relative increase during a GLE. For similar reasons the normalization value for the GLE spectrum is irrelevant when

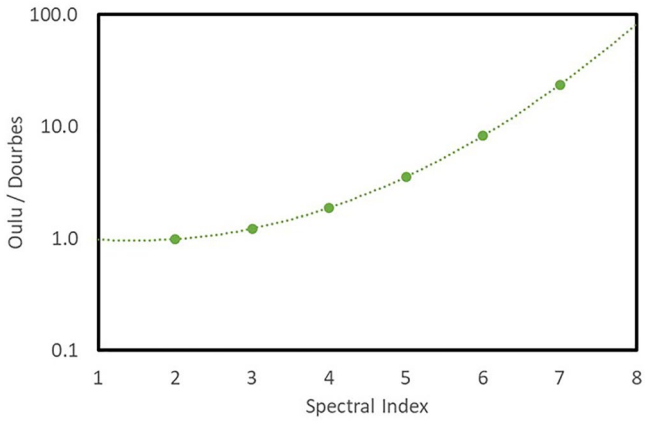

Figure 4. The ratio of predicted relative increases in count rate at Oulu and Dourbes neutron monitors as a function of spectral index. The dotted line shows a fit to points calculated for discrete values of spectral index.

comparing predicted increases at different locations. The calculated ratio of predicted count rate increases at Oulu and Dourbes is plotted against spectral index (γ) in Figure 4.

The spread in increase ratios, from ∼unity at low spectral index (where the slope at high rigidity/energy is similar to the GCR background) to >20 at a spectral index of 7, is of a sufficient range to have confidence that differences in real GLE spectral shapes would manifest themselves in a clearly resolvable way on this scale (assuming of course that the magnitude is sufficient to cause a measurable increase at both Oulu and Dourbes).

As shown in Figure 4, the discrete ratios have been fitted with a quadratic function in log-linear space that emulates the observed trend very successfully. This enables a conversion from observed increase ratio to spectral index using the following equation:

$$\gamma = \frac{\sqrt{b^2 - 4a\left(c - \ln\left(\frac{\Delta CR_{OULU}}{\Delta CR_{DRBS}}\right)\right)} - b}{2a} \quad (2)$$

where $\Delta CR_{[NM]}$ is the excess count rate of a neutron monitor above the normal GCR only count rate, $a = 0.1045$, $b = -0.3056$, and $c = 0.1794$.

Excess count rates in Oulu and Dourbes data are determined by comparison to the median count rate in the three hours before the onset of the GLE. The onset time is when the Oulu count rate exceeds a predetermined threshold (currently set at 8% above the median count rate from the preceding baseline). Having established the spectral index (γ) via this process, the next step is to calculate the normalization parameter (J_0 in Equation 1). This can be achieved using data from a single neutron monitor station, which should be the higher latitude one of the pair used to derive spectral index (Oulu in this case), as the increase is more statistically significant (we address what to do when a GLE triggers a measurable increase at Oulu but not at Dourbes in the next section). Extracting J_0 can be achieved by comparing the measured count rate increase at Oulu with the calculated increase based on multiplying ground level neutron spectra for the GLE (with arbitrary normalization) and the GCR background with the NM64 monitor response function. However, to further increase the rapidity of calculation, we explored the possibility of using integral neutron flux at ground level as a proxy for neutron monitor count rate. Figure 5 shows how this simpler approach compares to the full spectrum method, by calculating the relative "error" as a function of spectral index. Using a low threshold of 10 MeV, the relative error increases as a function of spectral index. This is because softer GLE spectra have a lower fraction of very high energy neutrons (>100 MeV), which contribute disproportionately to the count rate (Dyer et al., 2018), so the count rate increase is overpredicted. Conversely, when too high a flux threshold is used (e.g., 100 MeV), this same difference in neutron spectra leads to underprediction of the count rate at high values of γ (soft spectra). We find that an energy threshold of ∼60 MeV minimizes the discrepancy between the integral flux method and full spectrum method, with an average difference of only ∼3%. Therefore, we have implemented this method for rapid calculation of the GLE spectrum normalization parameter in MAIRE+.

3.2. Small/Soft Events

The MAIRE+ algorithm for GLE spectral index determination requires both Oulu and Dourbes neutron monitors to exhibit a measurable rise in count rate compared to the GCR background. The majority of historical GLEs are small and do not satisfy this criterion. However, as the greatest threat to aviation comes from larger events, this does not undermine the purpose of the model. Nevertheless, it is advantageous to include a fallback mode to be used when such a situation arises. A GLE that does not cause a significant increase at Oulu (failing to surpass our nominal 8% threshold e.g.,) is very unlikely to cause a large increase in dose rate (or neutron flux) at aviation altitudes in the skies over Northern Europe. However, it is possible for a GLE to cause a significant increase at Oulu *without* causing a significant increase at Dourbes. Given the relationship established in Figure 4 it is easy to evaluate the phase space for such an occurrence as a function of spectral index. Figure 6 shows how, for a situation

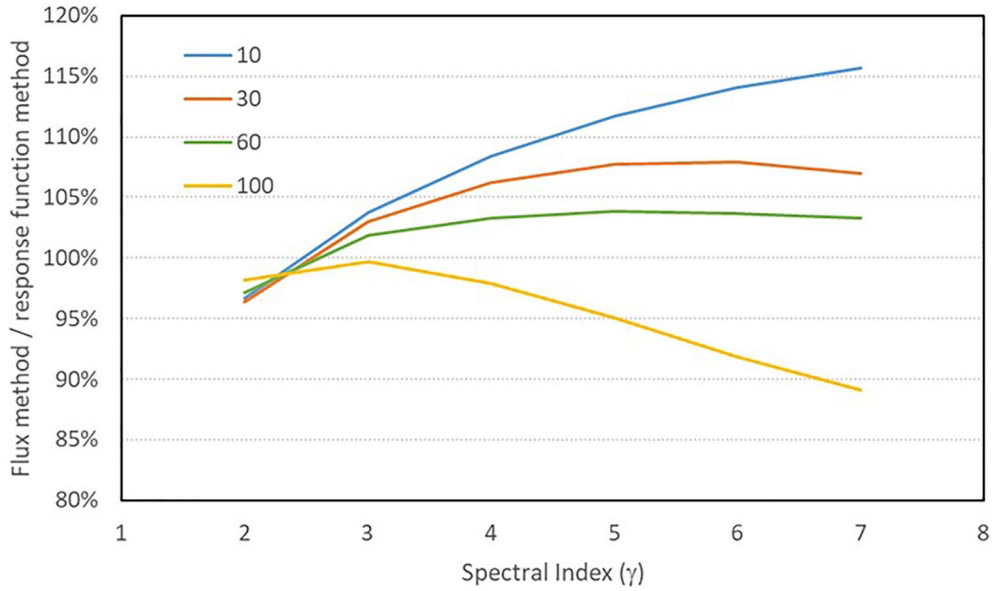

Figure 5. Ratio of normalization parameter, J_0, calculated using integral flux (threshold values in MeV are shown in the legend) to an alternative value based on count rates using the full neutron spectrum combined with a NM64 response function.

where there is no observed rise in count rate greater than 8% at Dourbes, the range of plausible values for spectral index decreases with the observed increase at Oulu.

This relationship imposes a constraint on the primary GLE spectrum when no significant increase is observed at Dourbes. This constraint in turn is of consequence for the range in possible dose rates at higher altitudes. Table 2 shows calculated effective dose rates at 9 km (30 kft) and 12 km (39 kft) for three representative scenarios of observed percentage increase in the count rate at Oulu. Effective dose rates are given as a function of spectral index, with the "forbidden" values according to Figure 6 left blank. The corresponding dose rates for the GCR background (in solar minimum) are 3.5 μSv/h and 7.8 μSv/h at 9 and 12 km, respectively. The cut-off rigidity is assumed to be zero for all these scenarios, as this represents the worst case and all GLE dose rates would be far lower at higher rigidity.

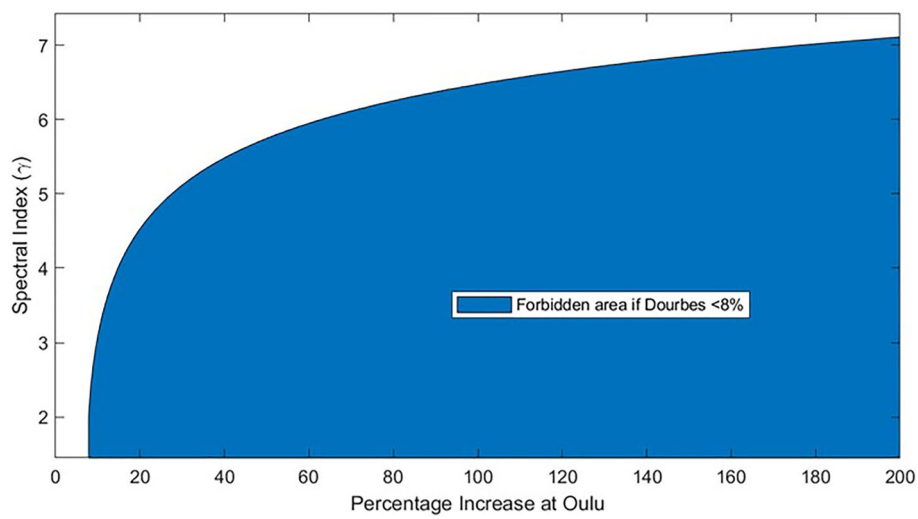

Figure 6. Illustration of "allowed" spectral index range as a function of percentage increase at Oulu, if the increase at Dourbes remains below 8%.

Table 2
Dose Rates at Aviation Altitudes (in Microsieverts per Hour) for Three Representative Percentage Increases at Oulu and the Corresponding "Allowed" Range in Spectral Index

	10% at Oulu		25% at Oulu		60% at Oulu	
GLE spectral index	9 km	12 km	9 km	12 km	9 km	12 km
2	-	-	-	-	-	-
3	0.5	1.3	-	-	-	-
4	0.7	2.3	-	-	-	-
5	1.01	3.6	2.5	8.9	-	-
6	1.4	5.2	3.4	13.0	8.1	31.2
7	1.8	7.6	4.5	18.9	10.7	45.5
GCR	3.5	7.8	3.5	7.8	3.5	7.8

Note. Cut-off rigidity is zero in all cases.

It is clear from these numbers that, while a lack of increase at Dourbes introduces some additional uncertainty into the dose rate calculation (via a reduced knowledge of the spectral shape), the spread in dose rates is limited by the reduced allowable range in spectral index as the event increases in magnitude. MAIRE+ adopts the conservative approach of assuming a realistic worst case for the aviation environment - which, for extrapolating upwards from ground data, is a soft spectrum with $\gamma = 7$. This value is used for all periods where the Oulu count rate is more than 8% above background and the Dourbes count rate is less than 8% above background. Although this risks overestimating the dose rate by a small amount in some circumstances, we note that this could only occur for small to moderate sized events and is consistent with a conservative safety approach to nowcasting the risk to aviation.

3.3. Trigger Mechanism

The requirement of an 8% increase in count rate observed at Oulu to trigger GLE calculation in MAIRE+ ensures that this mode should not be activated by random statistical fluctuations. We estimate that the 8% threshold, which is also used in relation to the Dourbes count rate to trigger spectral index determination using relative increases, corresponds approximately to a five-sigma statistical significance threshold (based on 5-min averaging). However, unphysical spikes in neutron monitor data are known to occur for assorted reasons relating to the collection and processing of data, and these also must be guarded against in terms of false triggering of the GLE calculation mode. To achieve this we use the wholly independent data source of proton flux measurements from the Solar and Galactic Proton Sensor (SGPS) on NOAA's GOES-16 geostationary spacecraft (Kress et al., 2020, 2021). NOAA's Space Weather Prediction Center (SWPC) provides real time data from this instrument, including differential and integral flux, every 5 min (https://www.swpc.noaa.gov/). NOAA's own space weather alert scale for radiation, the S-scale, is based on an integral flux above 10 MeV (Hanslmeier, 2002; Poppe, 2000) and is used to alert airlines to potentially enhanced dose rates at aviation altitudes. However, it is well-known that this energy threshold is too low for this application and can lead to multiple false alarms (Matthiä et al., 2009; Meier & Matthiä, 2014). Most solar particle events that lead to significant increases in >10 MeV proton flux in geostationary orbit do not also lead to GLEs. Relevance to GLEs requires a much higher energy threshold, commensurate with the production threshold for secondary particle cascades in the atmosphere.

We therefore use the highest available integral flux channel from SGPS (>500 MeV) as our coincidence trigger for the MAIRE + GLE mode. Figure 7 shows data from the west-facing SGPS instrument on GOES-16 (each spacecraft in the GOES-R series has two SGPS instruments, with the west-facing instrument having slightly better magnetic connection to interplanetary space), with the mean level and 50% above mean (i.e., a trigger threshold) illustrated with dashed lines. This very small GLE in October 2021 still resulted in a near doubling of the >500 MeV geostationary proton flux, which implies that any GLE of greater significance to the aviation environment would easily meet the 50% threshold GOES coincidence condition for triggering the GLE mode in MAIRE+. We note also that the 50% threshold corresponds to a flux of ~0.5 protons $cm^{-2}sr^{-1}s^{-1}$, and so this could be used as an alternative absolute threshold. This has the advantage of simplicity, but the disadvantage of not accounting for changes to the baseline during a Forbush decrease.

An example of why this additional safeguard against GLE false alarms is required can be found in the alert issued by the Athens neutron monitor system Anemos system (Mavromichalaki et al., 2018) on 5 November 2021. The GLE alert system was triggered by sharp rises in the count rates of three neutron monitors–SOPO and SOPB at the South Pole and Jungfraujoch in Switzerland. However, these rises were the result of an unusually rapid recovery in the count rate following a double Forbush decrease in the preceding 48 hr. Although this decrease and recovery was also observed in GOES >500 MeV flux data, the threshold of a 50% increase in flux was not met. Figure 8 shows how the magnitude of increase in count rate following the double Forbush decrease of early November 2021 is, for these locations, greater than the magnitude of the increase during GLE73 in late October. By contrast, the lower panel of Figure 9 shows how this is not the case for high energy GOES flux (in either the west-facing or east-facing detectors).

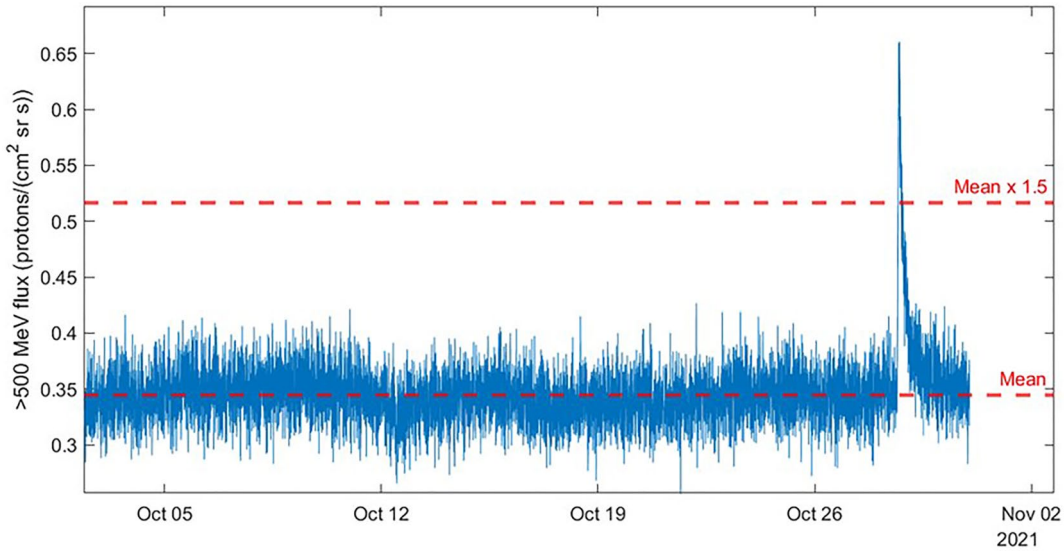

Figure 7. GOES-16 > 500 MeV proton flux (West-facing SGPS detector) from October 2021. A spike associated with GLE73 is visible on the right-hand side and horizontal red dashed lines show the mean (and 50% above the mean) of the period prior to the GLE.

Figure 9 shows that a Forbush decrease can occur before a GLE (as with GLE72 in September 2017) or after a GLE (as with GLE73 in October 2021). The data also show east - west asymmetry in the data, a phenomenon observed by the previous generation of GOES spacecraft (Rodriguez et al., 2010). The west-facing instrument (as used by MAIRE+) shows a greater increase in flux, but in all four cases (two instruments and two GLEs) the 50% increase threshold is met during the GLE but not during the recovery from Forbush decreases. This space-based

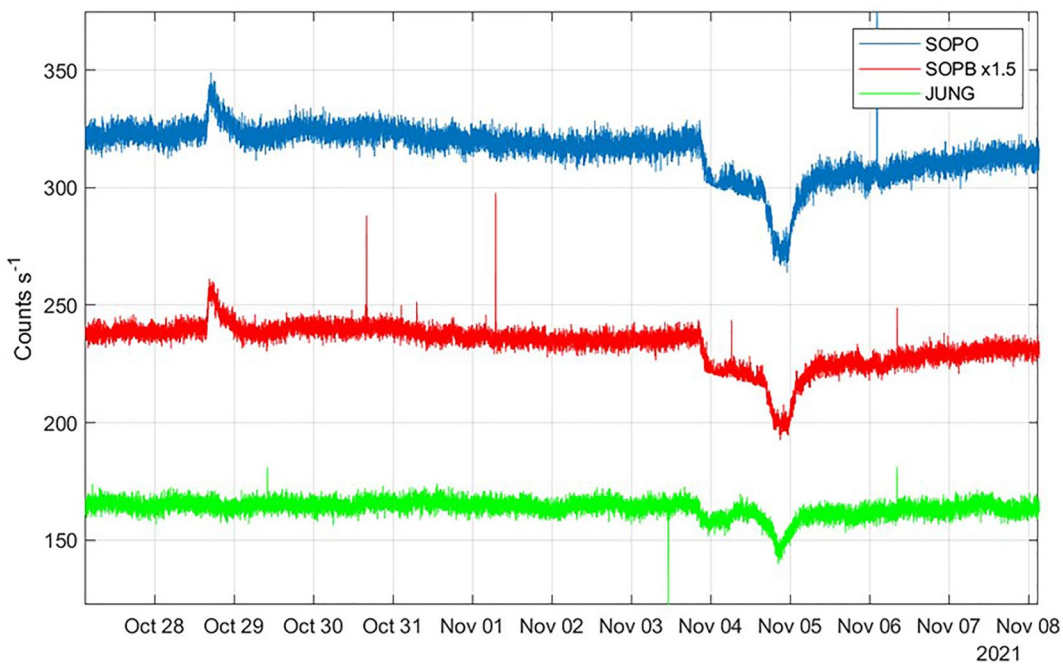

Figure 8. Neutron monitor data from SOPO, SOPB, and JUNG stations from 27 October to 9 November 2021 (NB SOPB count rate has been scaled by 1.5 for display purposes). The sharp increases observed on 5 November, which led to a false alarm GLE alert being issued, were greater in magnitude than the equivalent increases observed during GLE73 on 28 October.

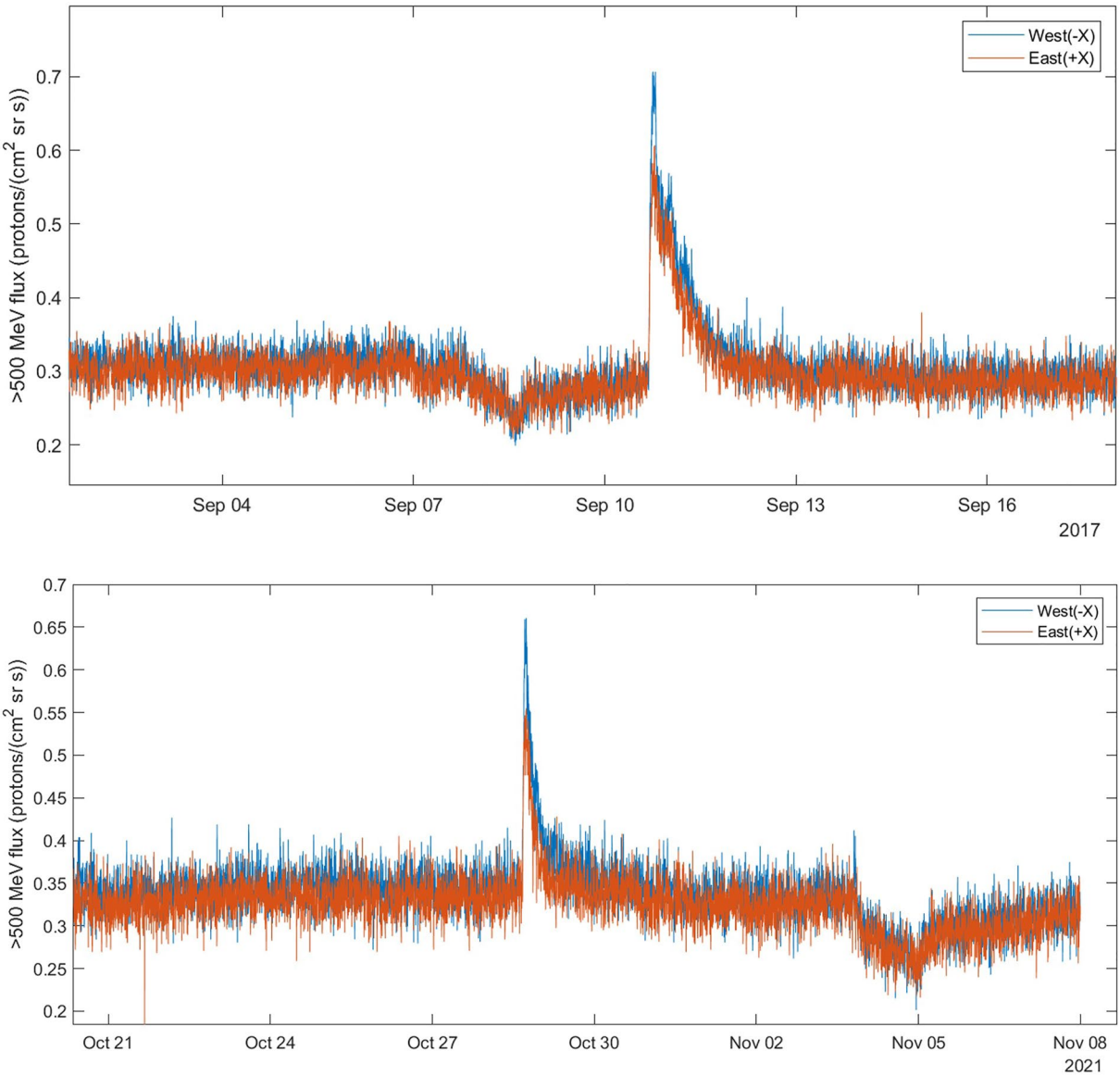

Figure 9. Examples of Forbush decreases preceding GLE72 (top panel) and following GLE73 (bottom panel) in both west-facing and east-facing SGPS detectors on GOES-16. East-West asymmetry is observed during both GLEs.

coincidence trigger therefore provides a necessary additional safeguard from false alarms and gives confidence that MAIRE+ outputs will maintain a high level of reliability during complex space weather conditions.

One potential drawback of using GOES data as a coincidence trigger in MAIRE+ is the potential for a delay in initiating GLE mode calculations due to a lag between the onset rise times of Oulu and GOES, respectively. It has been observed in previous events that neutron monitors may "see" the start of a GLE before GOES-based SWPC alerts are issued. This is in part due to velocity dispersion in Sun-Earth transit and in part due to early event anisotropy and the greater number of neutron monitor stations. We effectively negate the former effect by using the GOES channel with the highest available energy threshold (500 MeV), but we cannot avoid the latter. However, in order to circumvent this effect, we will allow MAIRE+ to begin GLE mode calculations based only on the Oulu (8%) trigger threshold, with GLE confirmation being triggered by GOES. Outputs during the interim period will be marked as "provisional" calculations, though in any large event this period is expected to be brief.

Once triggered, the GLE mode remains operational until Oulu count rates drop to less than 1.5% above the baseline. The value of the baseline remains fixed through the GLE mode operation, that is, it is always based on the

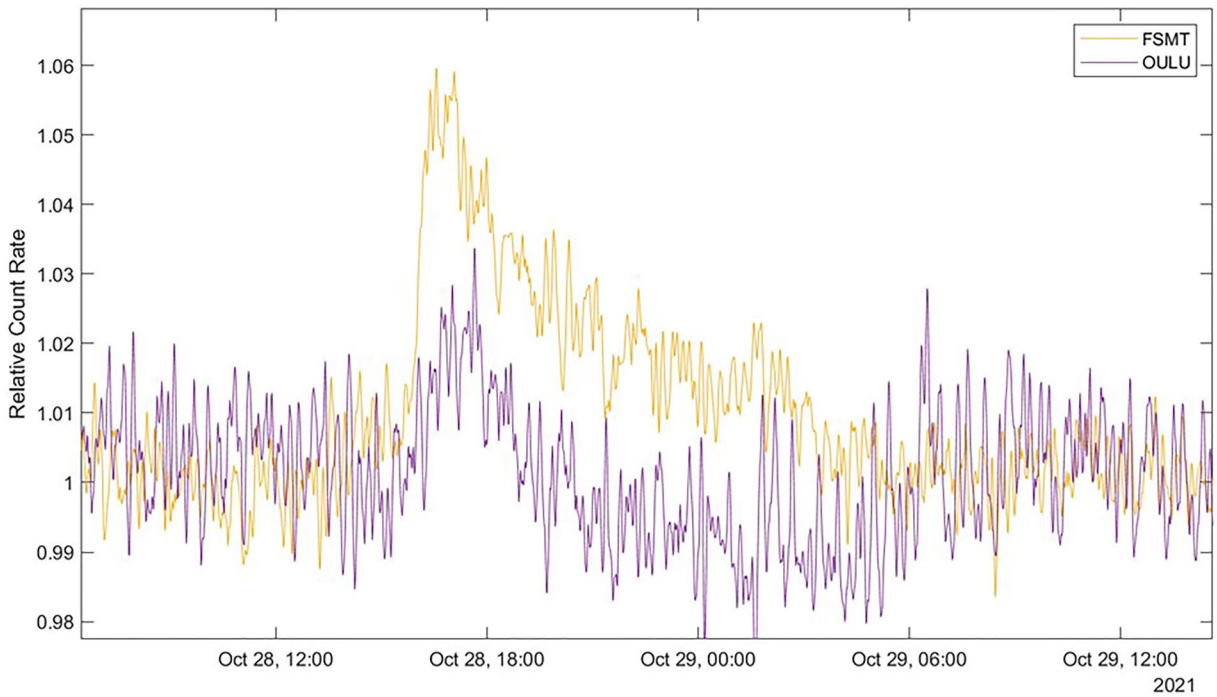

Figure 10. Relative count rates from Fort Smith (Canada) and Oulu (Finland) neutron monitors during GLE73.

two hours before the GLE mode is activated, regardless of the duration of the GLE. This ensures that the baseline is not affected by the progression of the event. If the GLE mode is using Oulu and Dourbes data for the spectral index calculation, but then Dourbes drops below the threshold of 1% above its pre-GLE baseline during the event, MAIRE+ uses the last calculated value of spectral index for the remainder of the event (i.e., until Oulu drops below 1.5% above baseline). If the increase at Dourbes never exceeds 8% of its pre-GLE baseline then the model defaults to a spectral index of 7.

4. GLE73

The most recent GLE (#73) occurred at approximately 16:00 on 28 October 2021. Only small increases were observed, predominantly at high altitude and high latitude stations such as SOPO (~5% increase at peak) and SOPB (~6% increase at peak). Slightly larger increases were observed at the high altitude mini-neutron monitors DOMB and DOMC, though with more uncertainty on the counting statistics. The largest observed increases at ground level were measured at similar levels to the South Pole high altitude stations, with Fort Smith and Peawanuck peaking at just over 5% above baseline (other Canadian monitors showed smaller increases however). Oulu peaked at just over 2% above the preceding baseline, thus MAIRE + GLE mode was not triggered, even though the model was operational at the time. A comparison between Oulu and Fort Smith is shown in Figure 10. By contrast, and as shown in Figure 9, GOES >500 MeV fluxes peaked at ~90% and ~60% above the preceding baseline, for west-facing and east-facing detectors, respectively.

Although the MAIRE + GLE mode was not triggered, we can estimate the increase in dose rates at flight altitudes based on Oulu data alone. Scaling from Table 2 (using a spectral index of 7) we calculate that a 2% increase at ground level corresponds to additional dose rates of 1.5 μSv/h and 0.36 μSv/h at high latitude and 12 and 9 km, respectively. This is equivalent to an increase in GCR background dose rate of ~20% at 12 km and ~10% at 9 km. Such small increases pose a negligible additional risk to passengers or avionics, so the absence of GLE mode triggering in MAIRE+ during this event is acceptable. If Oulu had responded to the GLE with the same amplitude of increase as Fort Smith, these estimates of additional dose rate would be 2–3 times higher This is still very small compared to GLEs of relevance to aviation, but it highlights the advantages of using regional data to counteract uncertainty due to anisotropy.

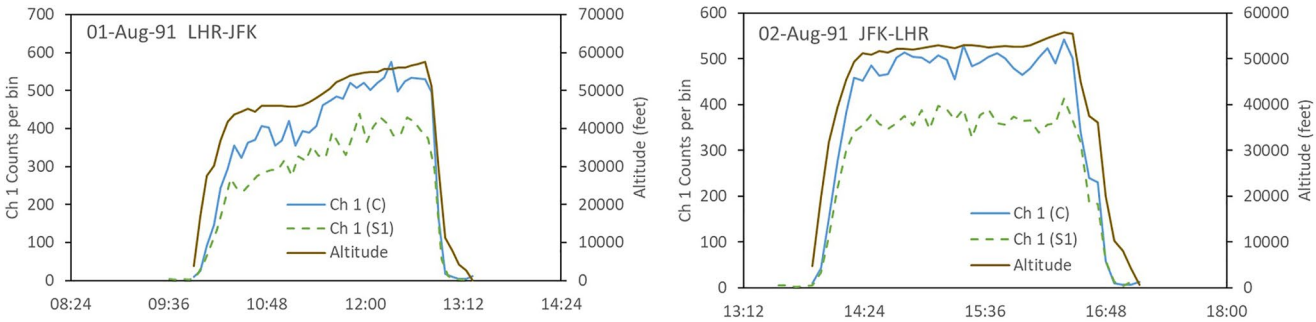

Figure 11. Channel 1 count rates for Concorde CREAM ("C") and Shuttle CREAM ("S1") on flights from LHR to JFK (LHS) and JFK to LHR (RHS). Altitude profiles are shown on the right hand scale in each case.

5. Validation of the Model With In-Flight Data

Calculations of GCR and GLE dose rates from MAIRE+ are only useful if they can provide reasonable estimates of the dose rates experienced on board aircraft. We have developed and deployed solid-state aircraft radiation detectors over several decades, covering wide varieties of flight altitudes and capturing periods of enhanced solar activity (Clewer et al., 2019; Dyer et al., 1990, 2007, 2009; Hands et al., 2016). These data provide a broad basis for comparing model outputs to measurements, and we aim to revisit these data sets for a more comprehensive assessment of MAIRE+. For the purposes of this article, which introduces the GLE model, we focus on the highly active period of September and October 1989 when four GLEs were observed by neutron monitors. These events were also observed by the CREAM monitor, which at the time was routinely deployed on the British Airways Concorde route between London Heathrow and New York JFK. Although some of these data have previously been published (Dyer et al., 1990, 2007), here we reexamine the calibration of the detector and use the capabilities of MAIRE+ to explore the CREAM dose profiles in more detail than has previously been possible. This unique data set of the largest GLEs ever measured in-flight enables a validation process for MAIRE+ outputs that has been unavailable for other similar models.

5.1. Instrumentation

The Cosmic Radiation Environment and Activation Monitor (CREAM) was initially developed as a radiation monitor for the Space Shuttle but was reconfigured as an integrated Concorde payload following the Challenger Space Shuttle disaster. Consisting of ten p-i-n diodes, each 1 cm^2 by 300 μm, CREAM measured the mixed-field aviation radiation environment through ionizing energy depositions in silicon (Dyer et al., 1989). Energy depositions are binned into 9 channels, which in the heavy-ion dominated space environment can be interpreted in the context of linear energy transfer (LET). In the aviation environment the interpretation of these channels is different. Lower channels are dominated by electron and proton direct ionization, whereas higher channels are dominated by indirect ionization by collisions between energetic secondary neutrons and protons with the silicon lattice (leading to both nuclear recoil and secondary ionizing products). Differences in count rates between the distinct Concorde CREAM and Shuttle CREAM detectors were observed during cross-calibration flights in 1991 and 1992, most likely due to varying depletion depths in the p-i-n diodes due to different applied reverse bias voltages. For example, Figure 11 shows count rate profiles for channel 1 on two CREAM units (C = Concorde, $S1$ = Shuttle 1) on two transatlantic Concorde flights in August 1991. The Concorde CREAM measured approximately 30% more counts than the Shuttle CREAM in channel 1, this ratio increases to an average of 50% in Channels 4–6 as the depletion volume ratio becomes more of a factor for indirect ionization. These comparisons are important as most ground-based calibration measurements were performed using the Shuttle version of the CREAM detector rather than the Concorde version that captured the 1989 GLEs.

We use C/S1 count rate ratios for "low LET" (Channel 1) and "high LET" (Channels 4–6) in conjunction with calibration data taken at the CERN-EU Reference Field (CERF) facility (Mitaroff & Silari, 2002) to infer ambient dose equivalent from Concorde CREAM count rates. The Shuttle CREAM units were cross-calibrated with tissue equivalent proportional counters (TEPCs) at CERF in 2006 and 2008 (Hands & Dyer, 2009) in order to establish dose coefficients for these monitors based on low LET and high LET TEPC counts in a mixed field environment.

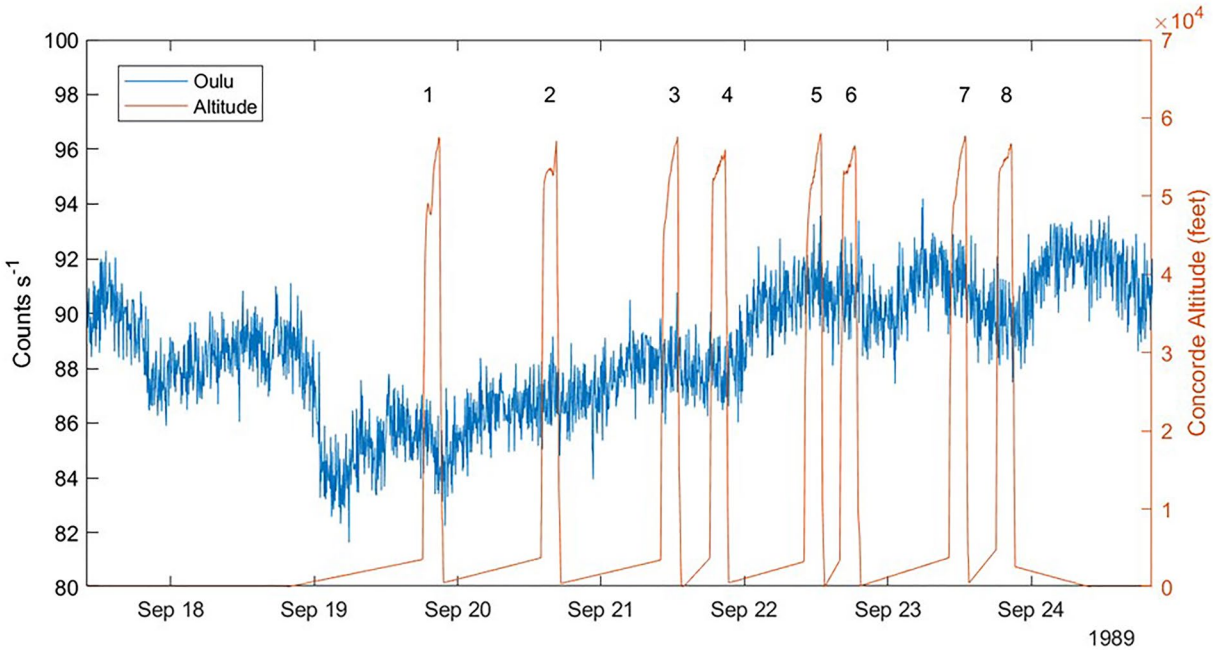

Figure 12. Oulu count rate (left axis) and altitude profiles for 8 Concorde flights (right axis) during a Forbush decrease in September 1989. Index numbers above each flight profile are used to reference these flights in the text.

Combining both CERF and flight calibrations we have calculated coefficients of 2,177 counts per micro-Sievert (low LET) and 13.0 counts per micro-Sievert (high LET) for the Concorde CREAM unit. These are applied to all subsequent calculations of ambient dose equivalent in this article.

5.2. Dose Rates in GCR Conditions

In September and October 1989, the CREAM Concorde unit was regularly flying between London and New York. Of particular interest are flights from mid-September, prior to the first GLE of this period (GLE42 on 29 September). Figure 12 shows eight flight altitude profiles from 19 to 23 September 1989, superimposed over the count rate of the Oulu neutron monitor. These flights clearly occurred during the recovery phase of a moderate Forbush decrease. Therefore, they provide an ideal testbed for the two GCR models embedded within MAIRE+, one of which (ISO) is guided by monthly sunspot number (and thus cannot reflect fluctuations on such a short timescale), while the other (DLR) is guided directly by the neutron monitor count rate (and thus can, albeit the model was designed to use monthly averaged count rates). Measured and calculated total route doses (in ambient dose equivalent) are plotted in Figure 13, while individual dose profiles are given in Figure 14 for the first (#1) and Figure 15 for the last (#8) in the series. Route dose numbers are given in Table 3.

These flights show the respective advantages and disadvantages of the two models in MAIRE+, at least in the context of these CREAM data. For flights #1 and #2, which take place before the cosmic ray background has recovered from the Forbush decrease, the ISO and DLR model, respectively, overpredict and underpredict the measured dose rate by a similar amount. By the end of the series, measured dose rates have increased to be much more in line with ISO model predictions (but are still divergent from DLR model predictions, even though these have also increased due to the dependence on Oulu count rate). Thus, MAIRE+ is better able to recreate the in-flight dose rate in quiescent conditions (away from Forbush decreases) using the ISO model, whereas using the DLR model enables MAIRE+ to reflect changes in the fine structure of the cosmic ray background during such short-term disturbances. Another way of putting it is that the ISO model is more successful in recreating absolute GCR dose rates during this period (for reasons discussed later in the paper) but, unlike the DLR model, it cannot recreate the relative changes during Forbush decreases.

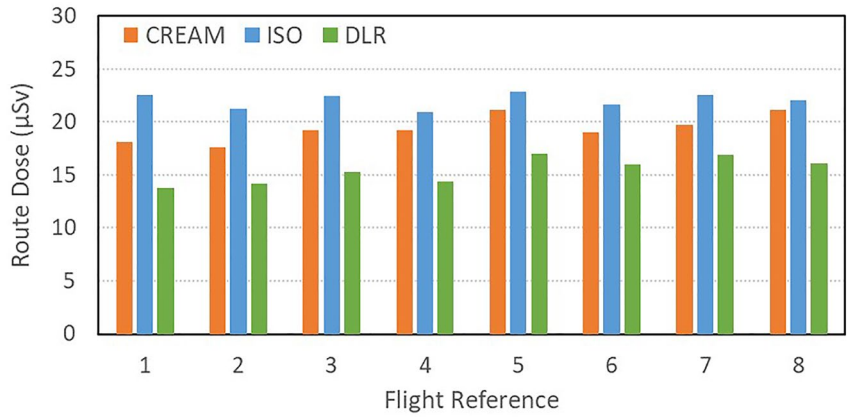

Figure 13. Route doses (in ambient dose equivalent, H*(10)) on eight transatlantic Concorde flights in September 1989, as measured by CREAM and calculated by MAIRE+ with ISO and DLR models for the GCR background, respectively.

5.3. Dose Rates in GLE Conditions

The modulation of cosmic ray intensity, though important, does not represent the greatest radiation hazard to avionics or passengers on board aircraft. During a so-called ground level enhancement, the enhancement factor in radiation intensity is of course far higher at aviation altitudes than on the ground. The International Electrotechnical Commission estimates that the factor increase in neutron flux during a large GLE (such as the largest

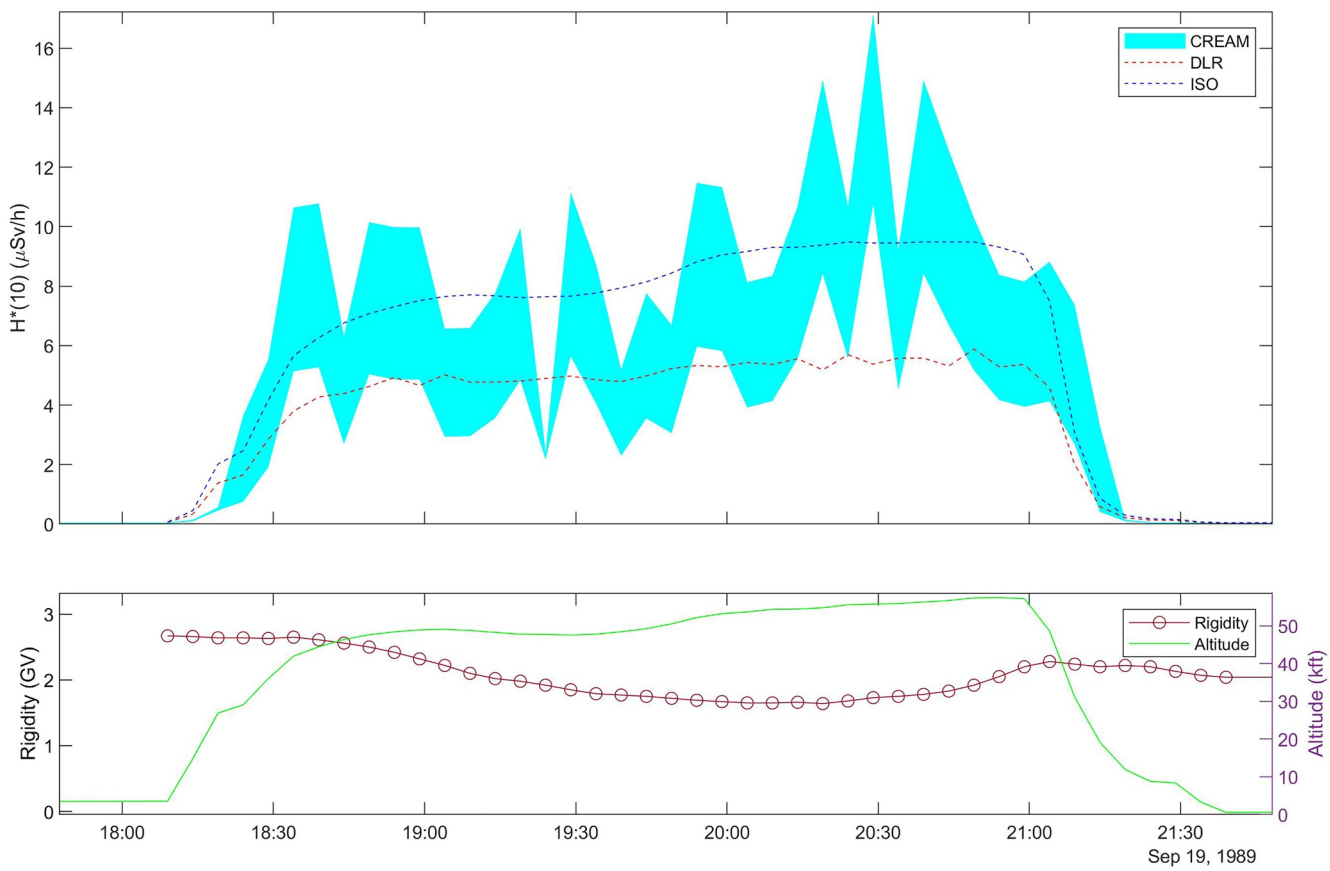

Figure 14. Flight dose profiles for flight #1 in Figure 12. The light blue shaded area shows the statistical uncertainty region for measured ambient dose equivalent rate (CREAM). Dashed red and dark blue lines in the upper panel show calculated GCR ambient dose equivalent rate according to DLR and ISO models respectively. The lower panel shows altitude and rigidity cut-off profiles for this LHR–JFK route.

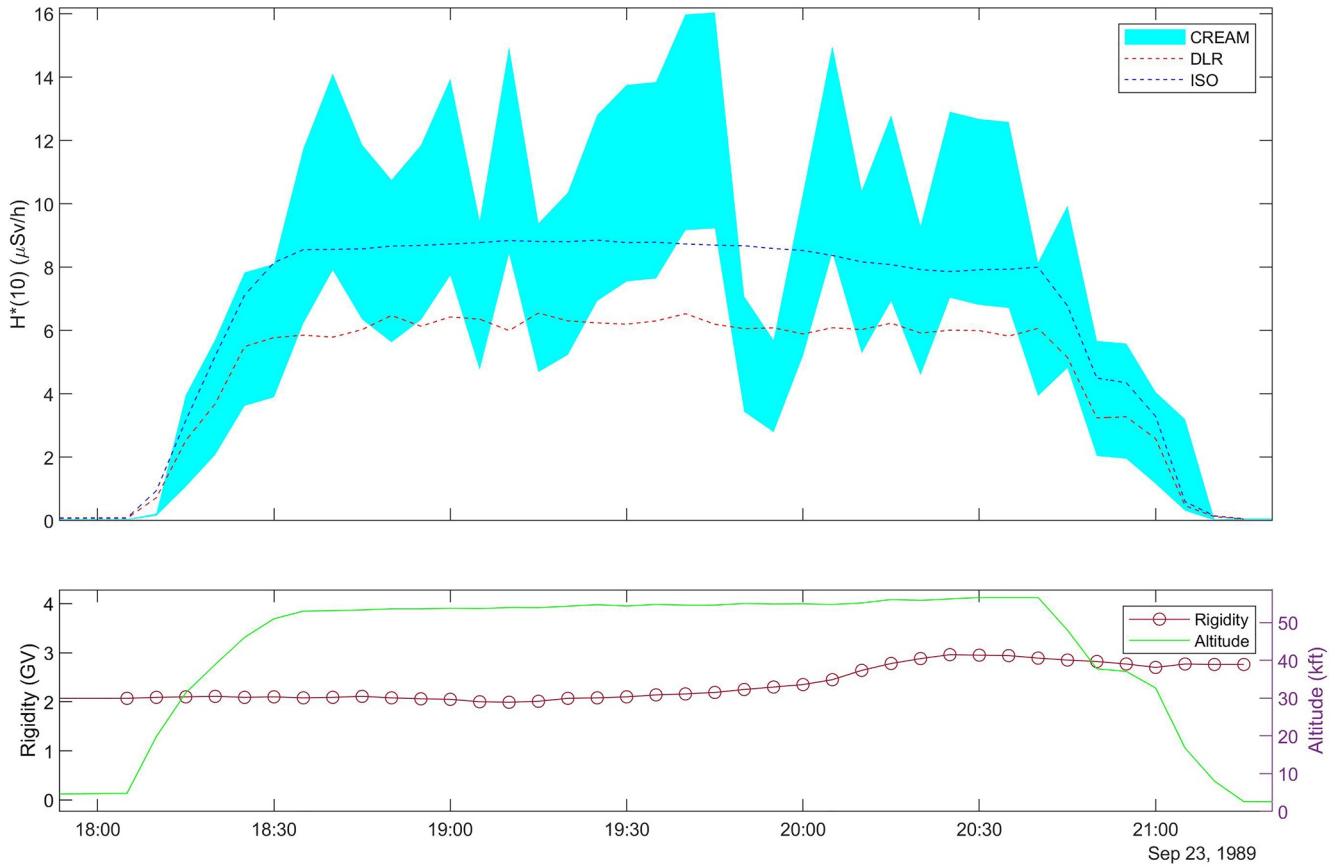

Figure 15. Flight dose profiles for flight #8 in Figure 12. The light blue shaded area shows the statistical uncertainty region for measured ambient dose equivalent rate (CREAM). Dashed red and dark blue lines in the upper panel show calculated GCR ambient dose equivalent rate according to DLR and ISO models, respectively. The lower panel shows altitude and rigidity cut-off profiles for this JFK–LHR route.

on record: GLE5 on 23 February 1956) is one thousand, with an additional factor of thirty applied in extremis if a one in a thousand year event is considered (Process management for avionics - Atmospheric radiation effects - Part 6: Extreme Space Weather, 2017). In such extreme cases, widespread failures of avionics systems may be expected, as well as ionizing doses to passengers greater than five millisieverts - equivalent to that of a full body medical scan and close to the recommended annual dose limit for European air crew (Dyer et al., 2018). MAIRE+ addresses both concerns by using representative single event effect cross sections (10^{-13} cm^2/bit for SEU and 10^{-8} cm^2/device for SEL, e.g., Dyer et al. (2006)) to output SEE rates as well as dose rates. In this article, we focus on dose rates for validation purposes due to the availability of empirical data. The Concorde CREAM detector was active in-flight during four GLEs in 1989 (GLEs 42–45). Using our updated calibration, in this section we present comparisons between these empirical data and outputs from MAIRE+. Figure 16 shows the five Concorde flights that coincided with GLEs in this period, as evidenced by the Oulu neutron monitor count rate.

Table 3
Route Doses (in Ambient Dose Equivalent, H(10)) on Eight Transatlantic Concorde Flights in September 1989, as Measured by CREAM and Calculated by MAIRE+ With ISO and DLR Models for the GCR Background, Respectively*

		Ambient dose equivalent (μSv)		
Reference	Route	CREAM	ISO	DLR
1	LHR–JFK	18.1	22.5	13.8
2	JFK–LHR	17.6	21.3	14.2
3	LHR–JFK	19.3	22.5	15.3
4	JFK–LHR	19.3	21.0	14.4
5	LHR–JFK	21.1	22.8	17.0
6	JFK–LHR	19.0	21.6	16.0
7	LHR–JFK	19.7	22.5	16.9
8	JFK–LHR	21.2	22.1	16.1

In MAIRE+, spectral index is determined from the ratio of relative increases in count rates between Oulu and Dourbes neutron monitors. In order to define the relative increases at each event it is necessary to define the baselines that such increases are measured against. In operational mode these are calculated every 5 min in real time. We provide the reference levels as they would have been calculated in 1989 in Table 4. An illustration of how spectral index evolves over time with the changing ratio of count rate increases at Oulu and

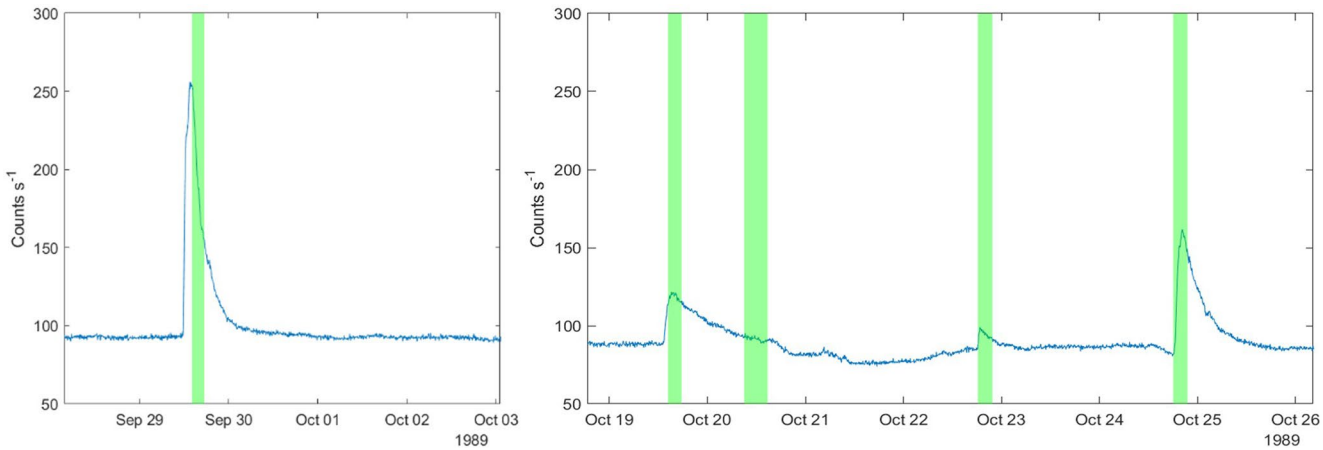

Figure 16. Concorde flight durations overlaid onto Oulu neutron monitor count rate. GLE42 is shown in the left plot and GLEs 43–45 are visible on the right plot. The flight on 20 October (during the tail end of GLE 43) includes a stopover in Bangor, ME.

Dourbes is shown in Figure 17. In this case, as with others, there is a little instability in spectral index at the start of the event due to the fast rise times in count rates. However, as the count rates peak and then decline, there is a clear pattern of an increasing spectral index (i.e., a softening primary spectrum) over the course of the event. This is qualitatively consistent with Figure 2 in Caballero-Lopez and Manzano (2022), where spectral index during GLE42 was obtained by comparing count rates from lead-free and conventional neutron monitors at the South Pole.

Primary spectra have been calculated in this way for the periods of the five Concorde flights shown in Figure 16 and then used to calculate ambient dose equivalent rates over the respective flight profiles. Results are shown in Figure 18 along with subplot displays of profiles for altitude, rigidity, Kp, and spectral index. For the second of these, depicting a JFK-LHR flight coincident with GLE43 on 19 October, precise route information was unavailable so we used latitude, longitude, and altitude values from the same route on 29 September.

There are many features to identify and discuss with respect to the different model options and comparisons to measured dose rates. The selection of cosmic ray model has a significant impact on both the GCR dose rate and the GLE dose rate (the latter because normalization of GLE spectra is based on quiescent >60 MeV flux, which in turn varies depending on GCR model). In this period, the ISO GCR model produces higher dose rates than the DLR model, as the latter is based on the quiescent Oulu count rate, which was particularly low during 1989. The relatively high solar maximum sunspot number also results in reduced GCR intensity, but not to the same extent. This can be seen most clearly in Figure 1 of Matthiä et al. (2013) by comparing solar cycles 21 (1976–1986) and 22 (1986–1997). The peaks of each cycle are very similar in terms of international sunspot number (ISSN), however, solar cycle 22 has a deeper minimum in Oulu count rate (thus a higher value of "W," which serves as a proxy for sunspot number in the model). This helps to explain the relatively low dose rates calculated by the DLR model during the 1989 GLEs, though a deeper investigation into the relative outputs of the two GCR models in MAIRE+ is planned for a future paper. It is important to note that the finer time resolution we use with the DLR model does not cause dose rates to be artificially lower in this period as Oulu count rates averaged over Bartels rotations (i.e., the timescale used to validate the model) are very similar to the pre-GLE baseline count rates we calculate with a 3 hr averaging period.

Table 4
Baseline Count Rates for Oulu and Dourbes Neutron Monitors During GLEs 42–45

		Baseline count rate (counts s^{-1})	
GLE #	Date	OULU	DRBS
42	29 September 1989	93.3	96.0
43	19 October 1989	88.4	92.1
44	22 October 1989	85.1	89.6
45	24 October 1989	82.6	86.6

The impact of GCR model choice is particularly noticeable during the flight on 20 October 1989, as here the GLE component is small (indeed it would be negligible were it not for the geomagnetic storm and high Kp reducing cut-off rigidities) during the tail end of GLE43. Using the DLR model produces dose rates that are significantly lower than those measured in the latter half of the flight, whereas using the ISO model produces much closer agreement (the remaining discrepancy at the end of the flight possibly implies underestimated GLE dose, which we discuss later).

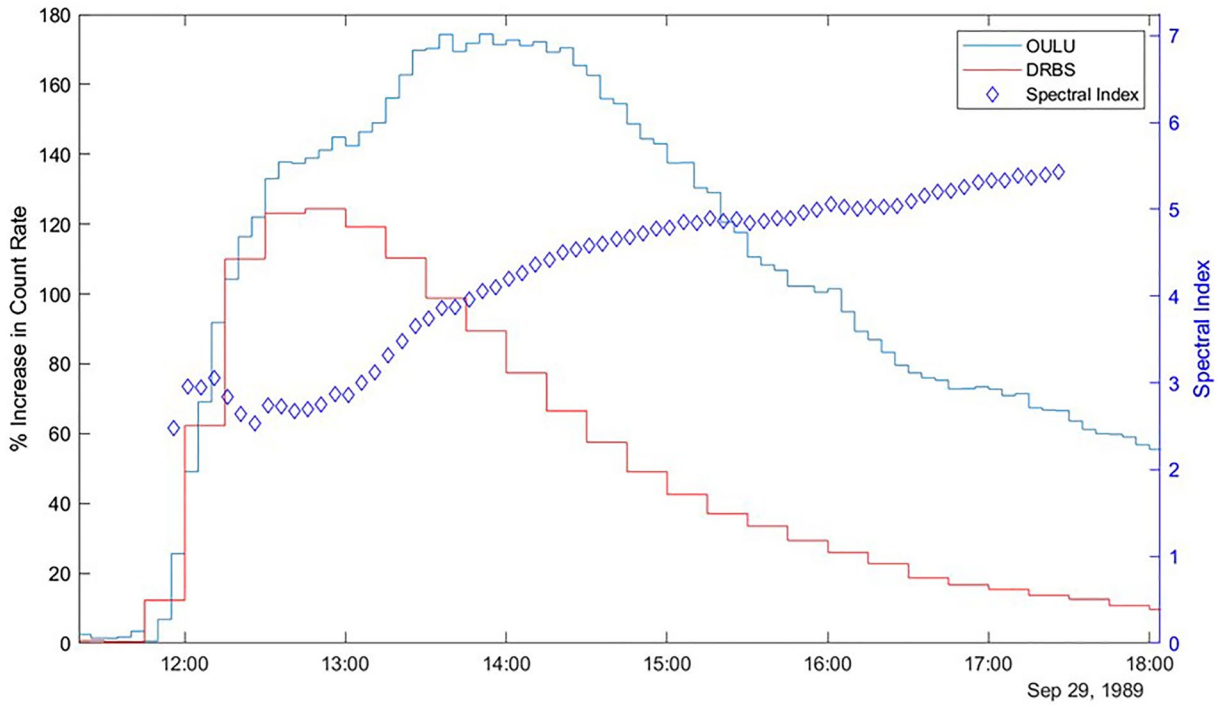

Figure 17. Relative increases in Oulu and Dourbes neutron monitor count rates (left scale) and the spectral index determined from the ratio by MAIRE+ (right scale) during GLE42.

The level of agreement between calculated and measured total dose rates varies from flight to flight. The greatest discrepancy occurs for the flight on 29 September 1989, during GLE42. Even using the ISO model the calculated total dose rate is less than half the measured rate at its peak. This is partly explained by a strong degree of anisotropy that was evident for this GLE. Increases observed by North American neutron monitor stations were significantly greater than their European counterparts, with the largest increase worldwide observed at the Calgary station (Lovell et al., 1998). As the Concorde flight took off from New York just after this event had begun, it should be expected that a West Atlantic neutron monitor profile would produce better results with respect to in-flight data. Figure 19 shows the impact of using the Calgary neutron monitor instead of Oulu to scale the GLE spectrum for GLE42 in MAIRE+, as well as alternative rigidity cut-off scenarios for GLEs 42 and 45 based on flight routes shown in Figure 20.

Figure 19 shows that using Calgary neutron monitor data instead of Oulu to scale the GLE spectrum intensity (with respect to GCR background) makes up about half the shortfall between MAIRE+ predictions and CREAM data. MAIRE+ is expected to evolve following initial implementation and we will explore adding the capability to reflect longitudinal anisotropy by using alternative pairs of neutron monitors to infer spectral index on a regional basis. This example based on the highly anisotropic GLE42 event implies that this approach would be highly beneficial. The other alternative dose profiles in Figure 19 use slightly tweaked flight routes (just 2° further north across the entire route and still lower latitude than the great circle path). The alternative rigidity profiles (dot-dashed red lines in Figure 19) show that the ΔR caused by this shift is of the order of 0.3–0.4 GV. The very steep gradient of dose rate versus rigidity for a GLE spectrum (which is significantly softer than the background GCR spectrum) is such that even this small change in cut-off rigidity is sufficient to cause more than a factor of two increase in calculated GLE dose rate, and thus can entirely close the gap between MAIRE+ calculations and CREAM measurements. Whether rigidity is the best explanation for the relatively small discrepancy between calculated and measured dose rates is open to question. It has been demonstrated before that even similar approaches for extrapolating ground-based data to dose rates at aviation altitudes can result in widely varying results with respect to each other and empirical data (Bütikofer & Flückiger, 2013, 2015). However, given that the vertical cut-off approximation we use does not account for primary particles arriving at different zenith angles, it is plausible that this is part of the explanation. It is known that the influence of zenith and azimuthal arrival direction has an impact on the effective cut-off rigidity at a given location (Storini et al., 2001), however, it is

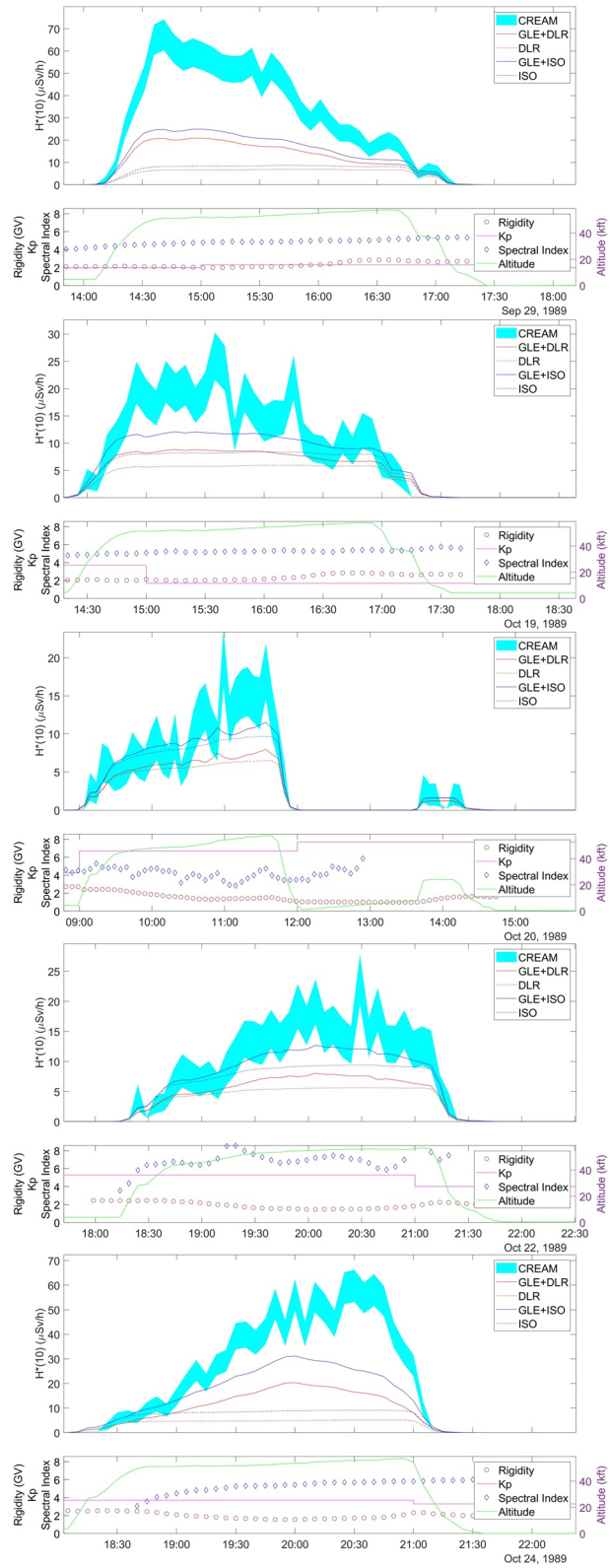

Figure 18. Measured and MAIRE+ calculated dose rates for five Concorde flights in September/October 1989. Ambient dose equivalent rates are shown in each top panel, with calculated components shown separately for Total (GLE + GCR) and GCR-only contributions (and for two different GCR models–ISO and DLR). Each lower panel shows flight altitude, Kp, geomagnetic cut-off rigidity, and derived spectral index.

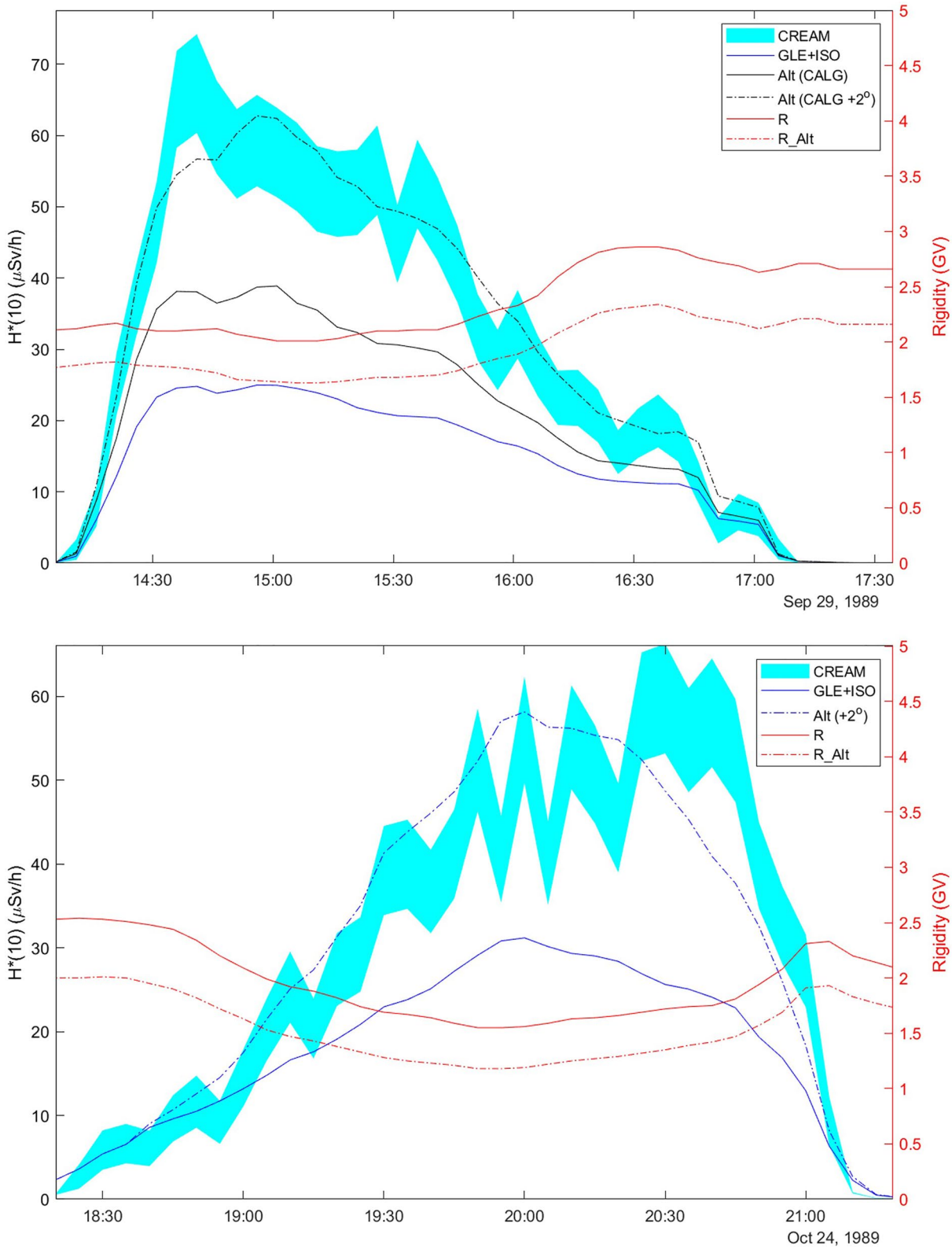
CREAM
GLE+ISO
Alt (CALG)
Alt (CALG +2°)
R
R_Alt
H*(10) (μSv/h)
Rigidity (GV)
14:30
15:00
15:30
16:00
16:30
17:00
17:30
Sep 29, 1989
CREAM
GLE+ISO
Alt (+2°)
R
R_Alt
H*(10) (μSv/h)
Rigidity (GV)
18:30
19:00
19:30
20:00
20:30
21:00
Oct 24, 1989

Figure 19.

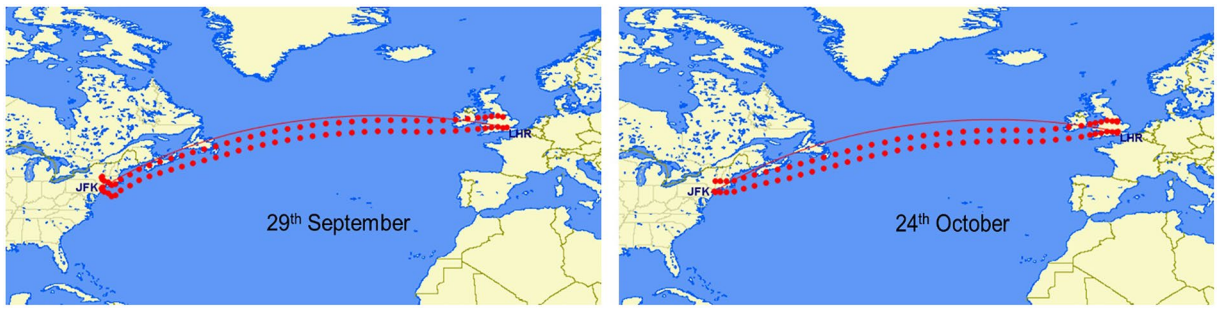

Figure 20. Flight routes used to calculate actual and alternative rigidity (and thus dose rate) profiles for GLE 42 on 29/09/89 (LHS) and GLE45 on 24/09/89 (RHS). Lower dotted lines are the actual flight routes, upper dotted lines are alternative flight routes (2° increase in latitude throughout) and the solid lines represent the great circle path. Images were created by Great Circle Mapper (gcmap.com).

nontrivial to include such effects in a real-time calculation of primary spectrum. Alternative explanations include further longitudinal anisotropy, systematic calibration effects with CREAM data and suppression of rigidity cut-off during geomagnetic storms (though Kp was only at two and 4, respectively, for GLEs 42 and 45, and this is taken into account by MAIRE+). Our calculations show that the strong geomagnetic disturbance during the tail end of GLE 43 (when the Kp index reached 8) approximately doubled the GLE dose rate, albeit from a low base. We aim to explore these issues further in future work.

Direct comparisons with the other flight dosimetry codes mentioned in this article have not been possible as they do not currently allow external users to run calculations with user-provided flight routes and historical data inputs. However, the ICAO Space Weather Service Coordination Group (ICAO/SWXCCG) has established a sub-team for the intercomparison of outputs from flight dosimetry codes used in the various ICAO space weather centers (including WASAVIES, AVIDOS, and CARI-7). Although MAIRE+ is not an official ICAO model, we aim to participate in this exercise so that outputs from our model can be compared to equivalent outputs from the models which drive ICAO space weather alerts directly. We plan to publish such comparisons in a future article reviewing the operational performance of MAIRE+ at the Met Office.

6. MAIRE+ Mapping Examples

Outputs from MAIRE+ have been converted into live display maps on a demonstration website (https://space-weather.surrey.ac.uk/). Global nowcast dose rate maps are available in terms of Effective dose (E), ambient dose equivalent (H*(10)), and dose equivalent, with different display mode options. An example of an effective-dose-rate map for the GCR background is shown in Figure 21. Dose rate maps are interactive and some transatlantic and transpolar flight route examples are shown projected onto zoomable polar-aspect subplots. Color displays can also be configured to reflect ICAO thresholds for "moderate" and "severe" radiation levels (Kauristie et al., 2021). Users can select an altitude from ground level up to 61 kft, with 3 km intervals above 25 kft. The grid size in latitude and longitude is 5°. All maps are updated every 5 min for both quiet and GLE periods.

The website also offers the capability of calculating dose rates over user-provided flight routes, based on a standard text file template. Current preloaded examples available on the flight route tool include Los Angeles–London Heathrow, New York–London Heathrow and Dubai–New York. A representative map showing the first of these examples is shown in Figure 22. This particular map shows dose rate but equivalent maps showing representative SEEs rates in avionics components are also available. This is a demonstration website only, the operational service hosted by the UK Met Office will use bespoke visualization that will be driven by the needs of trained space weather forecasters.

Figure 19. Alternative scenarios for calculated dose rate during GLEs 42 and 45. (LHS) CREAM data and MAIRE + GLE + ISO GCR dose rates are replotted from Figure 18. Also plotted are the MAIRE+ prediction using the Calgary neutron monitor to scale the GLE spectrum intensity (black curve) and this same method using a hypothetical flight path that is 2° further north in latitude throughout (in order to explore rigidity dependence). The rigidity profiles for the actual flight route and the alternative fight route are shown in solid and dashed red lines, respectively. (RHS) The same alternative (+2°) route scenario for GLE45 but retaining Oulu for GLE spectrum scaling as this event was more isotropic than GLE42. In all cases spectral index is determined by the Oulu/Dourbes count rate increase ratio.

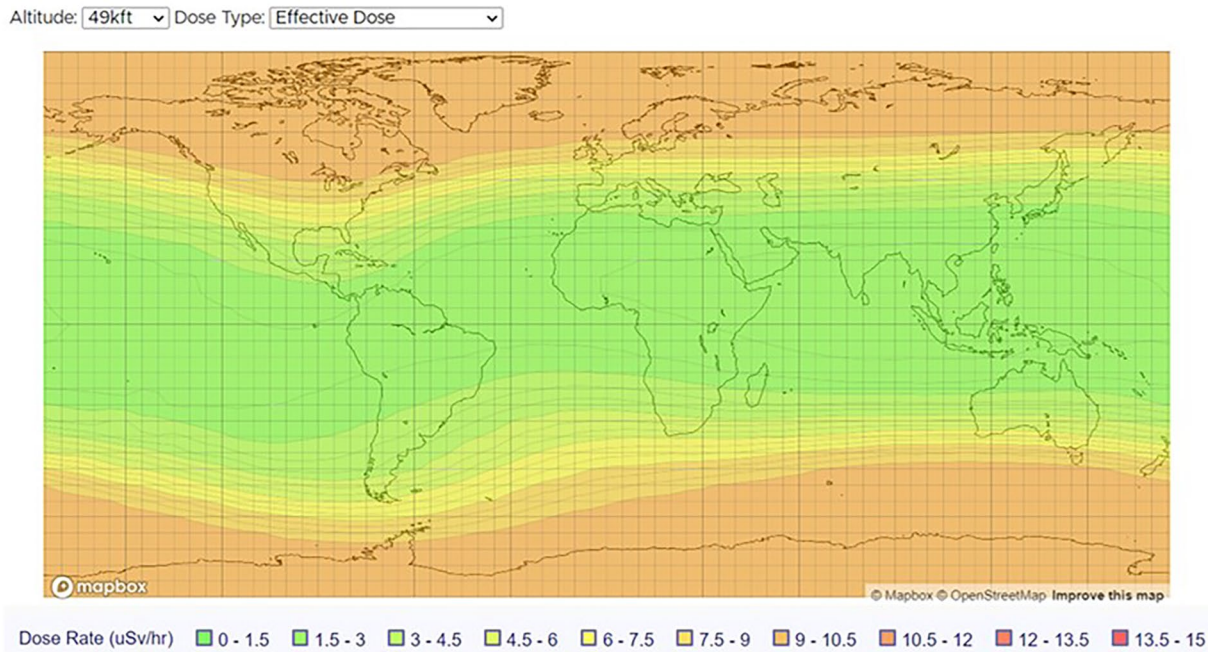

Figure 21. Global effective-dose-rate map during GCR background conditions at 49 kft.

7. Conclusions

The primary objective of this work is to provide real-time information on the global atmospheric radiation environment as a service to the airline industry, though it is also highly relevant to critical infrastructure at ground level. This service will be provided through the MAIRE+ model, with data from ground level neutron monitors as the primary driver. As the service will be hosted by the UK Met Office, with a remit covering the airspace near the UK, sourcing these inputs from Northern European neutron monitor stations is a sensible approach given known anisotropies in GLEs.

For the vast majority of time, MAIRE+ outputs will represent the background radiation environment created by GCR. In order to reflect short-term variations in this environment we have included a new GCR model developed by the German space agency, which uses Oulu neutron monitor data to modulate incoming cosmic ray intensity. The transport of these primary particles through the magnetosphere and the atmosphere is driven by precalculated response functions, though an additional data source of geomagnetic Kp index is also required to account for disturbances to the magnetosphere during geomagnetic storms. Using these inputs, MAIRE+ calculates dose rates and particle fluxes at all geographic coordinates and from ground level up to 20 km altitude. These quiet-time outputs can be used to monitor the exposure of air crew and passengers over the long-term, but they are not critical to short-term safety considerations.

To address the rapid increases in atmospheric radiation intensity that are associated with space weather (and are critical to short-term aviation safety considerations), we have developed an algorithm to derive primary input spectra, as a function of time, from the relative count rates of neutron monitors located in Finland (Oulu) and Belgium (Dourbes). Time-evolving primary GLE spectra are used to calculate radiation conditions in the atmosphere using exactly the same response functions as described for the GCR background. The GLE and GCR environments are summed to produce the total radiation environment during a space weather event. Outputs are configured to be consistent with ICAO space weather requirements, so that alerts based on “moderate” and “severe” enhancements to the radiation environment can be issued to aircraft.

In addition to neutron monitor data, MAIRE+ also ingests proton flux data from NOAA's geostationary GOES-16 spacecraft. The integral >500 MeV channel represents not only a good proxy for the galactic cosmic ray background but it is also a useful coincidence trigger for the GLE alert algorithm to avoid false alarms based on possible errors in real-time neutron monitor count rates. This improves the reliability of alerts from a model based

Figure 22. Flight route dose rate plotting tool on the MAIRE+ demonstration website.

on ground data but is no substitute for in situ data from in-flight monitors. We have performed initial validation with the best available data set of in-flight GLE measurements, though this is still limited in scope. Further validation of the GLE model depends on successfully capturing future GLEs in flight, which in turn depends on the widespread deployment of well-calibrated radiation monitors on a variety of flight routes. The large uncertainties revealed in this modeling work and that of others should be ample justification to pursue empirical campaigns using calibrated detectors, both to improve model development and to provide live space weather information to pilots.

MAIRE+ uses multiple data sources from instruments located on the ground in Europe and in geostationary orbit to nowcast the aviation environment for the aviation industry. Future work will focus on using additional data sources to improve the model's capability to reflect global anisotropies in the atmospheric radiation environment during space weather events. The possibility of using regional geomagnetic indices will also be explored in a future phase of the SWIMMR programme.

Data Availability Statement

GOES data are available online at https://www.ngdc.noaa.gov/stp/satellite/goes-r.html, hosted by NOAA's National Center for Environmental Information (NCEI). The data from the figures in this article are available at https://zenodo.org/record/6545717.

Acknowledgments
The SWARM project was funded by NERC (grant no. NE/V002899/1) under the SWIMMR programme, under the Strategic Priorities Fund (SPF) delivered by UKRI. We are grateful to the UK Met Office for supporting the development of the MAIRE+ model and hosting the outputs at MOSWOC. We acknowledge the NMDB database (www.nmdb.eu), founded under the European Union's FP7 programme (contract no. 213007) for providing data. We also specifically acknowledge the use of data from Oulu and Dourbes neutron stations, on which the MAIRE+ model is built. Oulu data are available at https://cosmicrays.oulu.fi/ and are supported by the Sodankyla Geophysical Observatory of the University of Oulu. Dourbes data can be viewed online at http://neutronmonitor.meteo.be/ and the operation of the neutron monitor is supported by the Royal Meteorological Institute of Belgium.

References

Alken, P., Thébault, E., Beggan, C. D., Amit, H., Aubert, J., Baerenzung, J., et al. (2021). International geomagnetic reference field: The thirteenth generation. *Earth Planets and Space*, *73*(1), 49. https://doi.org/10.1186/s40623-020-01288-x

Asvestari, E., Willamo, T., Gil, A., Usoskin, I., Kovaltsov, G., Mikhailov, V., & Mayorov, A. (2017). Analysis of Ground Level Enhancements (GLE): Extreme solar energetic particle events have hard spectra. *Advances in Space Research*, *60*(4), 781–787. https://doi.org/10.1016/j.asr.2016.08.043

Atwell, W., Tylka, A., Dietrich, W., Badavi, F., & Rojdev, K. (2011). Spectral analyses and radiation exposures from several ground-level enhancement (GLE) solar proton events: A comparison of methodologies. In *Paper presented at the 41st international conference on environmental systems*.

Band, D., Matteson, J., Ford, L., Schaefer, B., Palmer, D., Teegarden, B., et al. (1993). BATSE observations of gamma-ray burst spectra. I-Spectral diversity. *The Astrophysical Journal*, *413*, 281–292. https://doi.org/10.1086/172995

Battistoni, G., Cerutti, F., Fasso, A., Ferrari, A., Muraro, S., Ranft, J., et al. (2007). The FLUKA code: Description and benchmarking. In *Paper presented at the AIP Conference proceedings*.

Beck, P., Bartlett, D., Bilski, P., Dyer, C., Flückiger, E., Fuller, N., et al. (2008). Validation of modelling the radiation exposure due to solar particle events at aircraft altitudes. *Radiation Protection Dosimetry*, *131*(1), 51–58. https://doi.org/10.1093/rpd/ncn238

Boberg, P., Tylka, A., Adams, J., Jr., Flückiger, E., & Kobel, E. (1995). Geomagnetic transmission of solar energetic protons during the geomagnetic disturbances of October 1989. *Geophysical Research Letters*, *22*(9), 1133–1136. https://doi.org/10.1029/95gl00948

Bombardieri, D., Michael, K., Duldig, M., & Humble, J. (2007). Relativistic proton production during the 2001 April 15 solar event. *The Astrophysical Journal*, *665*(1), 813–823. https://doi.org/10.1086/519514

Bütikofer, R., & Flückiger, E. (2013). Differences in published characteristics of GLE60 and their consequences on computed radiation dose rates along selected flight paths. In *Paper presented at the journal of physics: Conference series*.

Bütikofer, R., & Flückiger, E. (2015). What are the causes for the spread of GLE parameters deduced from NM data? In *Paper presented at the journal of physics: Conference series*.

Caballero-Lopez, R., & Manzano, R. (2022). Analysis of the solar cosmic-ray spectrum during ground-level enhancements. *Advances in Space Research*. https://doi.org/10.1016/j.asr.2022.01.002

Clem, J. M., & Dorman, L. I. (2000). Neutron monitor response functions. In *Cosmic rays and Earth* (pp. 335–359). Springer.

Clewer, B., Ryden, K., Dyer, A., Hands, A., & Jackson, D. (2019). A citizen science network for measurements of atmospheric ionizing radiation levels. *Space Weather*, *17*(6), 877–893. https://doi.org/10.1029/2019sw002190

Copeland, K. (2018). *MIRA 2017: A CARI-7 based solar radiation alert system*. United States. Department of Transportation. Federal Aviation Administration. Office of Aviation. Civil Aerospace Medical Institute.

Danilova, O., Tyasto, M., Kananen, H., & Tanskanen, P. (1997). The cosmic ray asymptotic directions for station Oulu in the magnetic field of the Tsyganenko 1989 model. In *Paper presented at the international cosmic ray conference*.

Desorgher, L., Flückiger, E. O., & Gurtner, M. (2006). The planetocosmics geant4 application. In *Paper presented at the 36th COSPAR scientific assembly*. (Vol. 36, p. 2361).

Dyer, A., Hands, A., Ryden, K., Dyer, C., Flintoft, I., & Ruffenach, A. (2020). Single-event effects in ground-level infrastructure during extreme ground-level enhancements. *IEEE Transactions on Nuclear Science*, *67*(6), 1139–1143. https://doi.org/10.1109/tns.2020.2975838

Dyer, C., Hands, A., Ford, K., Frydland, A., & Truscott, P. (2006). Neutron-induced single event effects testing across a wide range of energies and facilities and implications for standards. *IEEE Transactions on Nuclear Science*, *53*(6), 3596–3601. https://doi.org/10.1109/tns.2006.886207

Dyer, C., Hands, A., Lei, F., Truscott, P., Ryden, K. A., Morris, P., et al. (2009). Advances in measuring and modeling the atmospheric radiation environment. *IEEE Transactions on Nuclear Science*, *56*(6), 3415–3422. https://doi.org/10.1109/tns.2009.2032185

Dyer, C., Lei, F., Hands, A., & Truscott, P. (2007). Solar particle events in the QinetiQ atmospheric radiation model. *IEEE Transactions on Nuclear Science*, *54*(4), 1071–1075. https://doi.org/10.1109/tns.2007.893537

Dyer, C., Sims, A., Farren, J., & Stephen, J. (1990). Measurements of solar flare enhancements to the single event upset environment in the upper atmosphere (avionics). *IEEE Transactions on Nuclear Science*, *37*(6), 1929–1937. https://doi.org/10.1109/23.101211

Dyer, C. S., Hands, A., Ryden, K., & Lei, F. (2018). Extreme atmospheric radiation environments and single event effects. *IEEE Transactions on Nuclear Science*, *65*(1), 432–438. https://doi.org/10.1109/tns.2017.2761258

Dyer, C. S., & Lei, F. (2001). Monte Carlo calculations of the influence on aircraft radiation environments of structures and solar particle events. *IEEE Transactions on Nuclear Science*, *48*(6), 1987–1995. https://doi.org/10.1109/23.983161

Dyer, C. S., Lei, F., Clucas, S., Smart, D., & Shea, M. (2003). Solar particle enhancements of single-event effect rates at aircraft altitudes. *IEEE Transactions on Nuclear Science*, *50*(6), 2038–2045. https://doi.org/10.1109/tns.2003.821375

Dyer, C. S., Sims, A. J., Farren, J., & Stephen, J. (1989). Measurements of the SEU environment in the upper atmosphere. *IEEE Transactions on Nuclear Science*, *36*(6), 2275–2280. https://doi.org/10.1109/23.45435

Hands, A., Baird, F., Ryden, K., Dyer, C. S., Lei, F., Evans, J., et al. (2021). Detecting ground level enhancements using soil moisture sensor networks. *Space Weather*, *19*(8), e2021SW002800. https://doi.org/10.1029/2021sw002800

Hands, A., & Dyer, C. (2009). A technique for measuring dose equivalent and neutron fluxes in radiation environments using silicon diodes. *IEEE Transactions on Nuclear Science*, *56*(6), 3442–3449. https://doi.org/10.1109/tns.2009.2034000

Hands, A., Lei, F., Ryden, K., Dyer, C., Underwood, C., & Mertens, C. (2017). New data and modelling for single event effects in the stratospheric radiation environment. *IEEE Transactions on Nuclear Science*, *64*(1), 587–595. https://doi.org/10.1109/tns.2016.2612000

Hands, A., Ryden, K., & Mertens, C. (2016). The disappearance of the pfotzer-regener maximum in dose equivalent measurements in the stratosphere. *Space Weather*, *14*(10), 776–785. https://doi.org/10.1002/2016SW001402

Hanslmeier, A. (2002). *The NOAA space weather scales* (pp. 193–200). The Sun and Space Weather.

Hatton, C., & Carimichael, H. (1964). Experimental investigation of the NM-64 neutron monitor. *Canadian Journal of Physics*, *42*(12), 2443–2472. https://doi.org/10.1139/p64-222

ISO. (2004). 15390: Space environment (natural and artificial) – Galactic cosmic ray model. *International Standard*.
Jiggens, P., Clavie, C., Evans, H., O'Brien, T., Witasse, O., Mishev, A., et al. (2019). In situ data and effect correlation during September 2017 solar particle event. *Space Weather*, *17*(1), 99–117. https://doi.org/10.1029/2018sw001936
Kananen, H., Tanskanen, P., Gentile, L., Shea, M., & Smart, D. (1991). A quarter of a century of relativistic solar cosmic ray events recorded by the Oulu neutron monitor. In *Paper presented at the international cosmic ray conference*.
Karapetyan, G. (2008). Detection of high energy solar protons during ground level enhancements. *Astroparticle Physics*, *30*(5), 234–238. https://doi.org/10.1016/j.astropartphys.2008.09.007
Kauristie, K., Andries, J., Beck, P., Berdermann, J., Berghmans, D., Cesaroni, C., et al. (2021). Space weather services for civil aviation—Challenges and solutions. *Remote Sensing*, *13*(18), 3685. https://doi.org/10.3390/rs13183685
Kress, B., Rodriguez, J., Boudouridis, A., Onsager, T., Dichter, B., Galica, G., & Tsui, S. (2021). Observations from NOAA's newest solar proton sensor. *Space Weather*, *19*(12), e2021SW002750. https://doi.org/10.1029/2021sw002750
Kress, B. T., Rodriguez, J. V., & Onsager, T. G. (2020). The GOES-R space environment in situ suite (SEISS): Measurement of energetic particles in geospace. In *The GOES-R series* (pp. 243–250). Elsevier.
Lantos, P., & Fuller, N. (2004). Semi-empirical model to calculate potential radiation exposure on board airplane during solar particle events. *IEEE Transactions on Plasma Science*, *32*(4), 1468–1477. https://doi.org/10.1109/tps.2004.830988
Latocha, M. (2018). Real time radiation dose assessment at civil flight altitudes due to galactic cosmic rays and spontaneous solar particle events. Retrieved from http://rifj.ifj.edu.pl/handle/item/283
Lei, F., Clucas, S., Dyer, C., & Truscott, P. (2004). An atmospheric radiation model based on response matrices generated by detailed Monte Carlo simulations of cosmic ray interactions. *IEEE Transactions on Nuclear Science*, *51*(6), 3442–3451. https://doi.org/10.1109/tns.2004.839131
Lei, F., Hands, A., Clucas, S., Dyer, C., & Truscott, P. (2006). Improvement to and validations of the QinetiQ atmospheric radiation model (QARM). *IEEE Transactions on Nuclear Science*, *53*(4), 1851–1858. https://doi.org/10.1109/tns.2006.880567
Lockwood, J. (1971). Forbush decreases in the cosmic radiation. *Space Science Reviews*, *12*(5), 658–715. https://doi.org/10.1007/bf00173346
Lockwood, J., Webber, W., & Debrunner, H. (1991). The rigidity dependence of Forbush decreases observed at the Earth. *Journal of Geophysical Research*, *96*(A4), 5447–5455. https://doi.org/10.1029/91ja00089
Lovell, J., Duldig, M., & Humble, J. (1998). An extended analysis of the September 1989 cosmic ray ground level enhancement. *Journal of Geophysical Research*, *103*(A10), 23733–23742. https://doi.org/10.1029/98ja02100
Matthiä, D., Berger, T., Mrigakshi, A. I., & Reitz, G. (2013). A ready-to-use galactic cosmic ray model. *Advances in Space Research*, *51*(3), 329–338. https://doi.org/10.1016/j.asr.2012.09.022
Matthiä, D., Heber, B., Reitz, G., Sihver, L., Berger, T., & Meier, M. (2009). The ground level event 70 on December 13th, 2006 and related effective doses at aviation altitudes. *Radiation Protection Dosimetry*, *136*(4), 304–310. https://doi.org/10.1093/rpd/ncp141
Mavromichalaki, H., Gerontidou, M., Paschalis, P., Paouris, E., Tezari, A., Sgouropoulos, C., et al. (2018). Real-time detection of the ground level enhancement on 10 September 2017 by A. Ne. Mo. S System Report. *Space Weather*, *16*(11), 1797–1805. https://doi.org/10.1029/2018sw001992
McCracken, K. (1962). The cosmic-ray flare effect: 1. Some new methods of analysis. *Journal of Geophysical Research*, *67*(2), 423–434. https://doi.org/10.1029/jz067i002p00423
Meier, M. M., & Matthiä, D. (2014). A space weather index for the radiation field at aviation altitudes. *Journal of Space Weather and Space Climate*, *4*, A13. https://doi.org/10.1051/swsc/2014010
Miroshnichenko, L. I. (2018). Retrospective analysis of GLEs and estimates of radiation risks. *Journal of Space Weather and Space Climate*, *8*, A52. https://doi.org/10.1051/swsc/2018042
Mishev, A., Kocharov, L., & Usoskin, I. (2014). Analysis of the ground level enhancement on 17 May 2012 using data from the global neutron monitor network. *Journal of Geophysical Research: Space Physics*, *119*(2), 670–679. https://doi.org/10.1002/2013ja019253
Mishev, A., Tuohino, S., & Usoskin, I. (2018). Neutron monitor count rate increase as a proxy for dose rate assessment at aviation altitudes during GLEs. *Journal of Space Weather and Space Climate*, *8*, A46. https://doi.org/10.1051/swsc/2018032
Mishev, A., & Usoskin, I. (2016). Analysis of the ground-level enhancements on 14 July 2000 and 13 December 2006 using neutron monitor data. *Solar Physics*, *291*(4), 1225–1239. https://doi.org/10.1007/s11207-016-0877-2
Mishev, A. L., Koldobskiy, S. A., Kovaltsov, G. A., Gil, A., & Usoskin, I. G. (2020). Updated neutron-monitor yield function: Bridging between in situ and ground-based cosmic ray measurements. *Journal of Geophysical Research: Space Physics*, *125*(2), e2019JA027433. https://doi.org/10.1029/2019ja027433
Mitaroff, A., & Silari, M. (2002). The CERN-EU high-energy reference field (CERF) facility for dosimetry at commercial flight altitudes and in space. *Radiation Protection Dosimetry*, *102*(1), 7–22. https://doi.org/10.1093/oxfordjournals.rpd.a006075
Normand, E. (1996). Single event upset at ground level. *IEEE Transactions on Nuclear Science*, *43*(6), 2742–2750. https://doi.org/10.1109/23.556861
Normand, E., & Baker, T. (1993). Altitude and latitude variations in avionics SEU and atmospheric neutron flux. *IEEE Transactions on Nuclear Science*, *40*(6), 1484–1490. https://doi.org/10.1109/23.273514
Nuntiyakul, W., Mangeard, P. S., Ruffolo, D., Evenson, P., Bieber, J., Clem, J., et al. (2020). Direct determination of a bare neutron counter yield function. *Journal of Geophysical Research: Space Physics*, *125*(4), e2019JA027304. https://doi.org/10.1029/2019ja027304
Nymmik, R., Panasyuk, M., Pervaja, T., & Suslov, A. (1992). A model of galactic cosmic ray fluxes. *International Journal of Radiation Applications and Instrumentation - Part D: Nuclear Tracks and Radiation Measurements*, *20*(3), 427–429. https://doi.org/10.1016/1359-0189(92)90028-t
O'Neill, P. M. (2010). Badhwar–O'Neill 2010 galactic cosmic ray flux model—Revised. *IEEE Transactions on Nuclear Science*, *57*(6), 3148–3153.
Paschalis, P., & Mavromichalaki, H. (2013). Optimization of neutron monitor data correction algorithms. *Nuclear Instruments and Methods in Physics Research Section A: Accelerators, Spectrometers, Detectors and Associated Equipment*, *714*, 38–47. https://doi.org/10.1016/j.nima.2013.02.031
Pelliccioni, M. (2000). Overview of fluence-to-effective dose and fluence-to-ambient dose equivalent conversion coefficients for high energy radiation calculated using the FLUKA code. *Radiation Protection Dosimetry*, *88*(4), 279–297. https://doi.org/10.1093/oxfordjournals.rpd.a033046
Petoussi-Henss, N., Bolch, W. E., Eckerman, K. F., Endo, A., Hertel, N., Hunt, J., et al. (2014). ICRP publication 116—The first ICRP/ICRU application of the male and female adult reference computational phantoms. *Physics in Medicine and Biology*, *59*(18), 5209–5224. https://doi.org/10.1088/0031-9155/59/18/5209
Plainaki, C., Mavromichalaki, H., Belov, A., Eroshenko, E., Andriopoulou, M., & Yanke, V. (2010). A new version of the neutron monitor based anisotropic GLE model: Application to GLE60. *Solar Physics*, *264*(1), 239–254. https://doi.org/10.1007/s11207-010-9576-6
Poppe, B. B. (2000). New scales help public, technicians understand space weather. *Eos, Transactions American Geophysical Union*, *81*(29), 322–328. https://doi.org/10.1029/00eo00247

Process management for avionics - atmospheric radiation effects - Part 6: Extreme space weather. (2017). Retrieved from https://webstore.iec.ch/publication/59928

Rodriguez, J., Onsager, T., & Mazur, J. (2010). The east-west effect in solar proton flux measurements in geostationary orbit: A new GOES capability. *Geophysical Research Letters*, *37*(7), L07109. https://doi.org/10.1029/2010gl042531

Sato, T., Kataoka, R., Shiota, D., Kubo, Y., Ishii, M., Yasuda, H., et al. (2018). Real time and automatic analysis program for WASAVIES: Warning system for aviation exposure to solar energetic particles. *Space Weather*, *16*(7), 924–936. https://doi.org/10.1029/2018sw001873

Shea, M., & Smart, D. (1990). A summary of major solar proton events. *Solar Physics*, *127*(2), 297–320. https://doi.org/10.1007/bf00152170

Storini, M., Smart, D., & Shea, M. (2001). Cosmic ray asymptotic directions for Yangbajing (Tibet) experiments. In *Paper presented at the international cosmic ray conference*.

Taber, A., & Normand, E. (1993). Single event upset in avionics. *IEEE Transactions on Nuclear Science*, *40*(2), 120–126. https://doi.org/10.1109/23.212327

Tsyganenko, N. A. (1989). A magnetospheric magnetic field model with a warped tail current sheet. *Planetary and Space Science*, *37*(1), 5–20. https://doi.org/10.1016/0032-0633(89)90066-4

Tylka, A. J., & Dietrich, W. F. (2009). A new and comprehensive analysis of proton spectra in ground-level enhanced (GLE) solar particle events. In *Paper presented at the 31th international cosmic ray conference*.

Usoskin, I., Ibragimov, A., Shea, M. A., & Smart, D. (2016). Database of ground level enhancements (GLE) of high energy solar proton events. In *Paper presented at the 34th international cosmic ray conference*.